Modelling the limits on the response of net carbon exchange to fertilization in a south-eastern pine forest

C.-T. LAI[1], G. KATUL[1], J. BUTNOR[2], M. SIQUEIRA[1,3], D. ELLSWORTH[1,4], C. MAIER[2], K. JOHNSEN[2], S. MCKEAND[5] & R. OREN[1]

[1]*Nicholas School of the Environmental and Earth Science, Box 90328, Duke University, Durham, NC 27708-0328, USA,* [2]*USDA Forest Service, Southern Research Station, 3041 Cornwallis Road, Research Triangle Park, NC 27707, USA,* [3]*Civil and Environmental Engineering, Duke University, Durham, NC 27708, USA,* [4]*School of Natural Resources and Environment, University of Michigan, 430 E. University, Ann Arbor, MI 48109-1115, USA and* [5]*College of Forest Resources, NC State University, Raleigh, NC 27695, USA*

ABSTRACT

Using a combination of model simulations and detailed measurements at a hierarchy of scales conducted at a sandhills forest site, the effect of fertilization on net ecosystem exchange (*NEE*) and its components in 6-year-old *Pinus taeda* stands was quantified. The detailed measurements, collected over a 20-d period in September and October, included gas exchange and eddy covariance fluxes, sampled for a 10-d period each at the fertilized stand and at the control stand. Respiration from the forest floor and aboveground biomass was measured using chambers during the experiment. Fertilization doubled leaf area index (LAI) and increased leaf carboxylation capacity by 20%. However, this increase in total LAI translated into an increase of only 25% in modelled sunlit LAI and in canopy photosynthesis. It is shown that the same climatic and environmental conditions that enhance photosynthesis in the September and October periods also cause an increase in respiration The increases in respiration counterbalanced photosynthesis and resulted in negligible *NEE* differences between fertilized and control stands. The fact that total biomass of the fertilized stand exceeded 2·5 times that of the control, suggests that the counteracting effects cannot persist throughout the year. In fact, modelled annual carbon balance showed that gross primary productivity (*GPP*) increased by about 50% and that the largest enhancement in *NEE* occurred in the spring and autumn, during which cooler temperatures reduced respiration more than photosynthesis. The modelled difference in annual *NEE* between fertilized and control stands (approximately 200 g C m^{-2} y^{-1}) suggest that the effect of fertilization was sufficiently large to transform the stand from a net terrestrial carbon source to a net sink.

Key-words: biosphere–atmosphere exchange; canopy carbon uptake; fertilization; net ecosystem exchange; turbulence modelling.

Correspondence: Ram Oren. Fax: +1 919 684 8741; e-mail: ramoren@duke.edu

INTRODUCTION

Over the past decade, several studies suggest that northern temperate forests can act as a large terrestrial sink for carbon (Ciais *et al.* 1995; Schimel 1995; Tans & White 1998; Houghton, Davidson & Woodwell 1998), and the pine forest of south-east USA is considered among the most productive among North American forests (Johnsen *et al.* 2001). However, these forests are generally situated at sites with moderate to poor soil fertility, which may limit their potential for carbon sequestration (Vitousek & Howarth 1991; Oren *et al.* 2001). Southern pine plantations, in particular, are typically nutrient limited (Pritchett & Smith 1975; Schultz 1997) and research has clearly shown productivity can be greatly enhanced by providing nutritional amendments (Albaugh *et al.* 1998; Samuelson *et al.* 2001).

When interpreting the effects of forest fertilization on net carbon uptake, it is necessary to evaluate the key processes observed from such experiments at their appropriate scale. At the leaf-scale, fertilization can increase photosynthetic capacity because the carboxylation capacity (V_{cmax}; please note all abbreviations are defined in Appendix C) increases with nitrogen content (Field & Mooney 1986; Evans 1989). Additionally, long-term fertilization increases the amount of photosynthesizing biomass because of increases in leaf area index (LAI; Brix & Ebell 1969; Vose & Allen 1988).

The commonly observed increase in LAI and total biomass with fertilization can induce several non-linear compensation effects that reduce net ecosystem carbon exchange (*NEE*) below values expected from leaf-level responses. Specifically, increased LAI will reduce the amount of photosynthetically active radiation (*PAR*) reaching deep in the canopy thereby reducing assimilation rates in the lower layers. Furthermore, fertilization increases several respiratory components and can significantly increase ecosystem respiration. Thus, fertilization typically enhances LAI and maximum photosynthetic rate, but it is not clear how the interplay between the canopy microclimate and the integrated photosynthetic and respiratory fluxes will affect *NEE*.

We examine the mechanisms responsible for *NEE* enhancement by fertilization using models and measurements collected at SETRES2 (South-east Tree Research and Education Site; McKeand *et al.* 2000). SETRES2 is a large-scale genotype×nutrition interaction experiment designed to quantify the effects of fertilization on the productivity of managed southern pine forests. A multilevel canopy photosynthesis-turbulent transport model, developed by Lai *et al.* 2000a, b), was used to simulate *NEE* for the fertilized and control stands for SETRES2. The model was independently tested with fluxes of sensible heat, latent heat, and *NEE* measured with eddy covariance (EC) over fertilized and unfertilized plots during a 3-week field campaign. The model was then employed to assess *NEE* and its components on monthly and annual basis.

MATERIALS AND METHODS

To quantify mass and energy exchanges between the vegetation and its microenvironment, a multilevel coupled photosynthesis-turbulent transport model, known as *CANVEG* after Baldocchi & Meyers (1998; see also Lai *et al.* 2000a, b), was developed and used. The model combines turbulent transport theory, eco-physiological and biochemical principles, radiation, and energy conservation regimes to predict mean source and flux distribution within the canopy from mean meteorological conditions above the canopy. The model differs from other multilevel photosynthesis models (e.g. Wang & Jarvis 1990; Collatz *et al.* 1991; Leuning, Denmead & Lang 1995; Williams *et al.* 1996) in that it resolves the entire canopy microclimate and incorporates feedbacks on biophysical sources associated with vertical variation in microclimate. Because the distribution of mean water vapour and carbon dioxide concentrations, or temperature within canopies are calculated, assumptions regarding the distribution of these state variables are not necessary. In

this application, the canopy height (h) was divided into N layers, each of thickness dz ($=0.5$ m), and all the equations and formulations described in the Appendices are solved iteratively at each discrete layer and for each 30 min time step. The model is driven by 30 min averaged air temperature ($\overline{T}_a$), water vapour ($\overline{q}_a$) and CO_2 ($\overline{C}_a$) concentration, mean wind speed ($\overline{U}$), *PAR*, leaf area density $a(z)$, soil heat flux (G_o) and soil temperature (T_{sl}) as shown in Fig. 1. Details about the model formulation can be found in Lai *et al.* (2000a, b). However, for completeness, we review the basic equations and required variables in Appendix A.

Study site

The experiment was conducted in a loblolly pine plantation adjacent to the SETRES2 study site in Scotland County of North Carolina, USA (34°48′ N, 79°12′ W). The stand, predominantly *Pinus taeda* L., was planted in 1993 at 1.5 m$\times2.1$ m spacing on an infertile, well-drained, sandy, siliceous, thermic Psammentic Hapludult soil (Wakulla series) with a water-holding capacity of 12–14 cm in a 2 m profile. Mean annual precipitation at this site is 1210 mm, evenly distributed throughout the year. Long-term mean air temperatures are 26 °C and 9 °C in the summer and winter, respectively. Sixteen 45 m×75 m plots were established at a randomized complete block design. Foliar nutrient ratios (Linder 1995) were used to guide annual fertilizer applications aimed at maintaining a balanced and optimal supply of all nutrients in the fertilized plots, so as to stimulate rapid growth (Allen 1987; Maier, Zarnoch & Dougherty 1998). The nitrogen treatment, approximately 11·2 g m^{-2} year^{-1} as urea, supplemented as necessary with other nutrients was similar to that described in Murthy *et al.* (1996) and Albaugh *et al.* (1998).

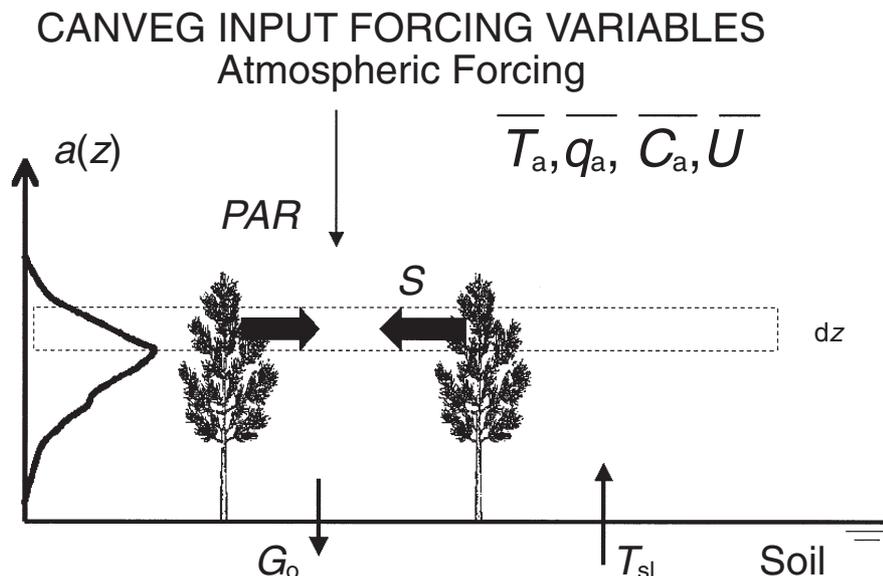Fluxes and environmental variables were measured separately for fertilized and unfertilized (control) stands using

Figure 1. Schematic display of the multilevel *CANVEG* model. The forcing variables required in *CANVEG* are also shown.

a mobile tower setup. The experiment was initiated on 23 September and data were collected over the fertilized stand until 3 October 2000. The system was then moved to the control stand and data collection was continued from 3 to 13 October 2000. This experimental period was chosen to coincide with warm soil temperatures and maximum LAI. Thus, if photosynthesis or respiration response to fertilization is large, the effect on *NEE* would be readily discernible during this period.

Eddy covariance flux measurements

The turbulent fluxes of sensible heat (F_T), latent heat (F_q) and CO_2 (F_c) above the canopy were measured with a conventional eddy covariance system consisting of an open path CO_2/H_2O gas analyser (LI-7500; LI-COR Inc., Lincoln, NE, USA) and a triaxial sonic anemometer (CSAT3; Campbell Scientific Inc., Logan, UT, USA). The sonic anemometer also provided the mean wind speed ($\overline{U}$) and other flow statistics for the scalar transport calculations. The system was mounted on a customized telescoping mast, which is an integral part of a mobile laboratory (Wolf Coach Inc., Auburn, MA, USA). The mobile laboratory is hydraulically levelled and guide wires were used to minimize mast vibration.

The open path gas analyser used is a non-dispersive infrared analyser measuring simultaneously CO_2 (C_a) and water vapour (q_a) concentration. The internal high-speed scan rate (150 Hz) was digitally filtered to permit a true high frequency response (up to 20 Hz bandwidth). The analyser was pre-calibrated in the laboratory prior to the experiment. The heads of both sensors were at the same height and approximately 10 cm from each other to minimize instrument separation corrections. The sampling rate was at 10 Hz, and all the data were transmitted by sequential digital measurement connection (Campbell Scientific Inc.) to avoid any lag or time delay. All signals were processed by a datalogger (CR23X; Campbell Scientific Inc.). The averaging interval for computing all turbulent fluxes was 30 min. The measured F_q and F_c were adjusted for density variations due to sensible heat using the standard Webb–Leuning correction (Webb, Pearman & Leuning 1980; Leuning *et al.* 1982).

Meteorological measurements

In addition to the EC flux measurements above the canopy, a Ta/RH probe (HMP45C; Campbell Scientific Inc.) was installed at $z = 15.6$ m to measure mean air temperature and relative homidity, where z is the height above the forest floor. The vapour pressure deficit (D_v) was computed from the latter measurements. A Fritchen-type net radiometer and a quantum sensor (Q7 and LI-190SA; LI-COR Inc.) were positioned to measure net radiation (R_n) and *PAR* above the canopy. Five soil heat flux plates (HFT3; Campbell Scientific Inc.) were installed in a grid within the footprint of the net radiometer to measure soil heat flux and

assess energy closures. All the meteorological measurements were sampled at 1 s and averaged over a 30 min period.

Footprint analysis

Due to the limited size of the experimental plots, an extensive footprint analysis on the EC measurements was necessary. Figure 2 shows the location of the EC system and the dominant wind direction over the sampling period. To ensure that the measurements were conducted in the atmospheric surface layer (ASL), the measurement height of the EC system was set at $z = 15.6$ m (≥ 2 h). The fact that EC measurements were conducted in the ASL greatly simplifies the estimation of the footprint or source weight function. The latter analysis was conducted using the model of Hsieh, Katul & Chi (2000), in which the peak location of the footprint (x_c) for different stability conditions was computed. Based on this analysis, we found that 63% of the runs collected at the fertilized stand were of flux originating within the stand ($>90\%$ of source identified); about 51% of runs at the control stand were of local flux.

A more direct evaluation of potential influence on flux measurements over one treatment by flux originating from the other treatment is to quantify biases in the relationship between measured water vapour fluxes (F_q) against net radiation measurements. Here, the expected differences in F_q between the treatments should be large due to the large difference in LAI, which would infuse bias into the R_n–F_q relationship for runs with an uncertain source footprint. The EC runs for which 90% of the computed source area is within the representative plot were related to their respective R_n measurements. We found that $<5\%$ of the EC measurements deviated significantly from the expected R_n–F_q slope in each treatment. Furthermore, the difference in slopes between the two treatments was significantly larger than the difference in slopes between measurements whose source contribution was uncertain, collected over the same stand ($P < 0.05$).

As a final test of how well the EC measurements taken at each measurement period represent mostly one treatment, we calculated the one-dimensional energy balance closure for fertilized and control stands and found that they were within 16% ($R^2 = 0.91$) and 3% ($R^2 = 0.93$), respectively. Combining this diagnosis with the footprint analysis, we conclude that 95% of the EC measurements in each period represent the intended treatment. These flux measurements were used to validate *CANVEG* model calculations for both stands.

Plant area density measurements

The mean canopy heights for fertilized and unfertilized plots were 6.8 ± 0.5 and 4.1 ± 0.5 m, respectively, at the time of the experiment. The vertical profile of plant area index (PAI, the leaf area plus branches) was measured at 1 m intervals from the top of the canopy to 1 m above the
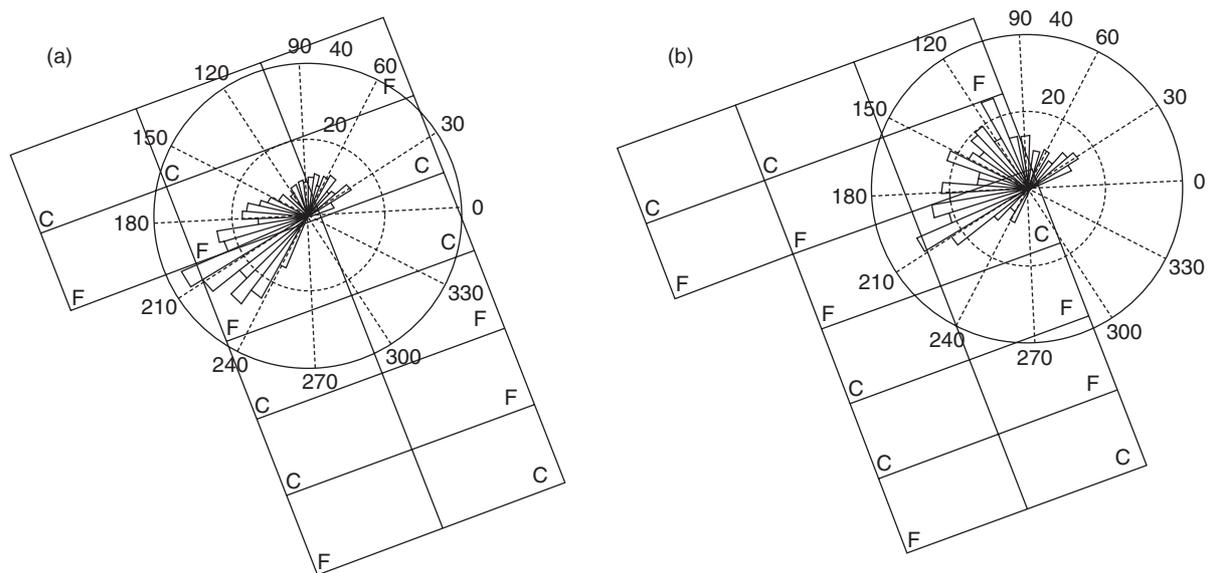
Figure 2. Placement of the mobile tower and the dominant wind direction measured at (a) the fertilized (F) and (b) the control (C) stands during the experiment. The centre of the polar coordinate plot is the location of the tower. Also shown is the wind direction histogram (blocks) relative to the North (0°) and the number of runs from each wind direction (shown as radii).

ground by gap fraction techniques following the theory described in Norman & Welles (1983). A pair of optical sensors with hemispherical lenses (LAI-2000; Li-Cor) was used in each of the two stands in Fig. 2 for canopy light transmittance measurements, from which gap fraction and plant area densities were calculated.

Leaf gas exchange measurements

Leaf level physiological parameters were determined from porometric measurements using a portable infrared gas analyser for CO_2 and H_2O (Li-6400 portable photosynthesis system; Li-Cor) and an integrated gas CO_2 supply system. The data were collected for upper canopy foliage at $z = 0.95\,h$ under sunny conditions, at a constant leaf temperature (28 °C). The A–C_i curves were measured and used to determine V_{cmax} and J_{max} using a least-square regression procedure described in Wullschleger (1993), where A is photosynthesis and C_i is the leaf-level intercellular CO_2. Needles were collected following gas exchange measurements and analysed for total nitrogen content after combustion based on the Dumas technique (NA-1500; Carlo-Erba Strumentiazone, Milan, Italy). The measured leaf nitrogen content (N_a) near the canopy top was 2·35 and 3·02 g m^{-2} projected leaf at the control and fertilized plots, respectively. The dependency of V_{cmax} on nitrogen content was then determined using the measurements conducted on the same foliage. Figure 3 shows that the data from the two treatments fell along the same positive linear relationship between leaf V_{cmax} and N_a established for this species at Duke Forest (Ellsworth, unpublished results). This relationship was therefore used in this study for modelling V_{cmax} and J_{max} to drive the *CANVEG* calculation of CO_2 flux. The physiological parameters of the stomatal conductance
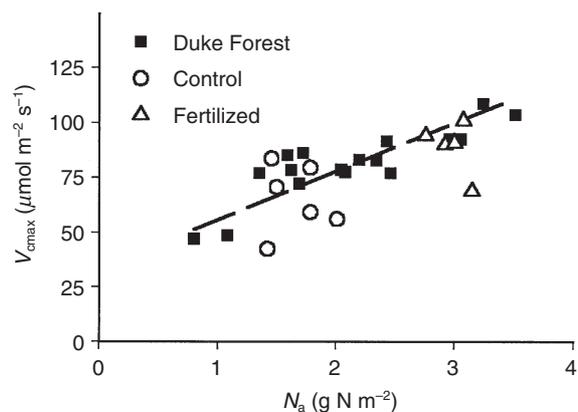

Figure 3. Relationship between maximum leaf carboxylation capacity (V_{cmax}) and leaf nitrogen content measured at $z/h = 0.95$.

model of Collatz *et al.* (1991) were also determined from these gas exchange data (see Lai *et al.* 2000b). All measured gas exchange rates are reported on a unit projected leaf area basis.

To estimate V_{cmax} at different canopy levels, we assumed that maximum N_a was at the canopy top, and attenuate the measured N_a value down the LAI profile following the approach described in Hirose & Werger (1987). According to Hirose & Werger (1987), the distribution of foliar nitrogen concentration within the canopy volume is given by:

$$N_a(z) = N_a(h) \exp(-K_o \xi)$$

where ξ is defined using relative cumulative leaf area index, and K_o is the nitrogen attenuation coefficient equivalent to the light attenuation coefficient (≈ 0.52 in this study) estimated from our light attenuation calculation (Campbell &

Norman 1998). Sampson & Allen (1998) showed that in loblolly pine plantations, a $K_o = 0.5$ is reasonable. Such distribution of $N_a(z)$ is now widely used in different types of canopies, and agrees well with measurements from other experiments (Field 1991; Leuning *et al.* 1995). Figure 4 shows the modelled *PAR* attenuation and the vertical distribution of $N_a(z)$ within the canopy; the latter was strictly used to estimate the vertical distribution of $V_{cmax}(z)$ based on the relationship in Fig. 3. We emphasize that the differences between measured and modelled $N_a(z)$ would lead to minor differences in $V_{cmax}(z)$, at least when compared to the scatter shown in Fig. 3.

Respiration measurements

Soil respiration R_{sl} was measured with a custom-designed, chamber-based system – Automated CO_2 Efflux System (ACES). ACES is a multiport, dynamic gas sampling system that utilizes an open flow-through design to measure

carbon dioxide fluxes sequentially from up to 15 chambers using a single infrared gas analyser (EGM-3; PP Systems Inc., Hertfordshire, UK) integrated into the system. Each chamber is equipped with a pressure equilibration port, ensuring that the chamber pressure was held near ambient (Fang & Moncrieff 1996; Maier & Kress 2000). Each chamber is sampled for 10 min to ensure steady-state conditions, and a value of R_{sl} was recorded on the tenth minute of the cycle. Nine complete runs (135 values) are recorded every day. When not being actively sampled, all chambers are continuously supplied with ambient air to prevent CO_2 build-up. Four plots (two fertilized and two control) were sampled concurrently using four ACES units, beginning two days before the eddy covariance monitoring commenced and ending 2 days after the monitoring was completed. In each plot, soil CO_2 efflux was measured with 13 chambers, and woody respiration was measured with two chambers, resulting in 26 chambers per treatment measuring soil CO_2 efflux, and four chambers per treatment mea-
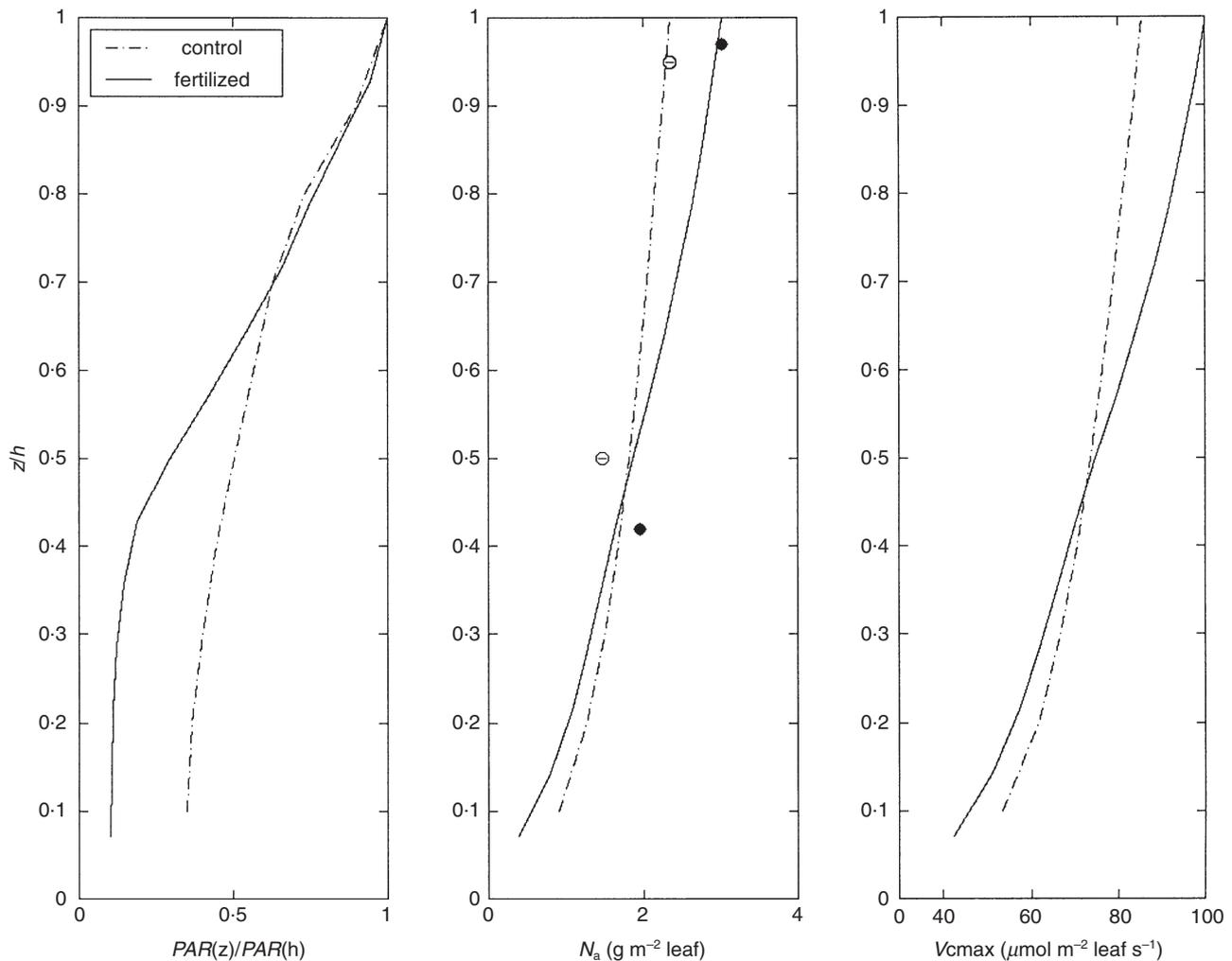

Figure 4. Modelled *PAR* attenuation, modelled $N_a(z)$ and computed $V_{cmax}(z)$ within canopy for control and fertilized stands. The symbols are measured leaf nitrogen at the control (open circles) and fertilized (closed circles) stands.

suring woody respiration. Detailed specification of the characteristics and operation of the two chamber types are provided below.

Soil component

Soil chambers (25 cm in diameter, i.e. 490 cm^2, 10 cm height) were placed on the forest floor with litter left intact. To ensure the measured R_{sl} is not biased by root density distribution, chambers of each ACES system were placed in the following manner: trees within the sampling area of the respiration units were randomly selected to receive a chamber, chambers were then randomly placed into one of the four position zones as shown in Fig. 5. The azimuth bearing from the tree was also randomly selected. We regressed measured R_{sl} with simultaneously measured T_{sl} to obtain a R_{sl}–T_{sl} response curve for each chamber, then averaged the coefficients of R_{sl}–T_{sl} curves situated at the same zone (see Fig. 5). Finally, a representative R_{sl}–T_{sl}

curve for the block was generated by weight-averaging the coefficients of R_{sl}–T_{sl} curve from each zone based on the ground area covered by that zone. The resulting R_{sl}–T_{sl} function is shown in Table 1 for both fertilized and unfertilized stands.

Above-ground component

We estimated stem respiration by measuring CO_2 efflux from stem segments into respiration chambers. Chambers were constructed of Teflon film attached to the stem using closed-cell foam collars positioned below the first live branch (approximately 0·5 m). Aluminium foil covered the Teflon film to exclude light and to prevent chamber warming. All chambers were 23·5 cm in length. Air volume within the chambers ranged from 825 to 1733 cm^{-3} depending on stem diameter (9·5–17·0 cm). Air entered and exited the bottom and top of the chamber, respectively, via Teflon diffuser rings. Chamber air and cambium temperatures
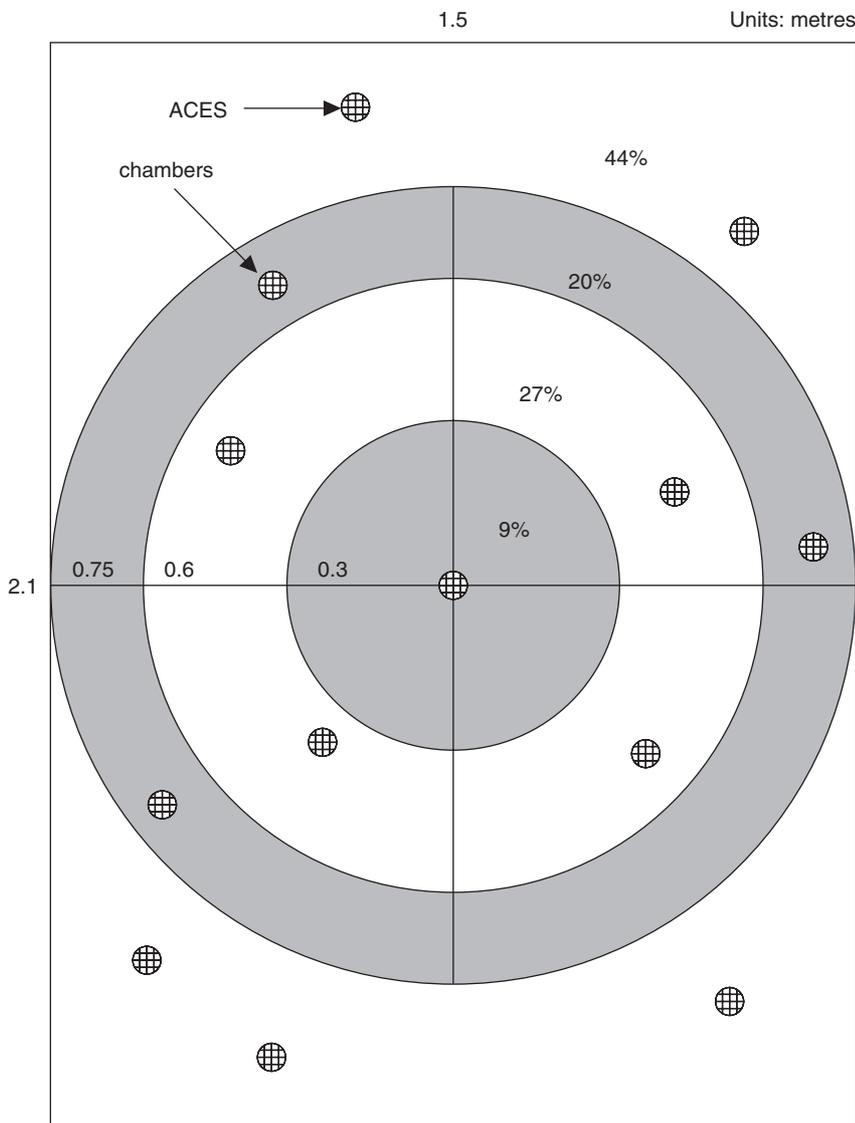

Figure 5. Schematic display of the placement of chambers connected to the Automatic Carbon Efflux System (ACES). The percentage of ground area covered by each zone and an example of chamber arrangement are shown.

Table 1. Eco-physiological and canopy attributes used in the *CANVEG* model for the period in September–October 2000. The forest floor respiration-to-temperature (R_{sl}–T_{sl}) response function from chamber measurements is: $R_{sl} = \kappa_1 \exp(\kappa_2 T_{sl})$, where R_{sl} is in $\mu mol\ m^{-2}\ s^{-1}$, and T_{sl} is soil temperature (°C). The above-ground woody respiration (R_w, $\mu mol\ CO_2\ m^{-3}\ s^{-1}$) was estimated from $R_w = \omega_1 + \omega_2 \times (V_w) \exp(\omega_3 T_w)$, where V_w is woody volume (m^3), and T_w is bole temperature (°C)

Variables	Control	Fertilized
LAI ($m^2\ m^{-2}$)	1·65	3·51
Characteristic leaf length		0·001
Leaf absorptivity for *PAR*, α		0·83
Clumping factor, Ω		0·8
Foliar N @$z/h = 0.95$ ($g\ m^{-2}$ leaf)	2·35	3·02
V_{cmax} @$z/h = 0.95$ ($\mu mol\ m^{-2}$ leaf s^{-1})	85·4	100·2
Stomatal slope parameter, *m*		7·5
Stomatal intercept parameter, *b*		0·015
Coefficients of R_{sl}–T_{sl} curve		
κ_1	0·728	0·322
κ_2	0·069	0·121
Estimated woody biomass V_w ($m^3\ ha^{-1}$)	38·3	88·4
Coefficients of R_w equation		
ω_1		−0·0146
ω_2		70·1049
ω_3		0·041

were measured simultaneously using thermocouples constructed from 24-gauge copper–constantan wire. Airflow rates were sufficiently high to ensure well-mixed conditions within the chamber. Stem respiration measurement was included as part of the ACES sampling cycle of soil respiration.

At the conclusion of the study, we measured stem diameter within each of the chambers. Above-ground woody respiration (R_w) was modelled as a function of cambium temperature (T_w) and the enclosed stem volume including bark (V_w). The equation used to estimate R_w was summarized in Table 1. The coefficients were calibrated specifically for this study via a multiple regression analysis (Maier *et al.* 1998).

To estimate V_w for the stand, tree height must be known. Height was measured on all trees annually and, beginning in year three, breast height diameter was also measured. Using locally developed allometric equations (McKeand *et al.* 2000), individual tree volume (stem and branches) was calculated, summed for the plot, and converted to per volume unit ground area. Canopy woody biomass data was not available for the exact time of the measurement campaign. To estimate the woody biomass for the end of year 2000 growing season, we used the measurements collected over the pervious three years (1997–99) and generated a linear relationship (least-square regression approach) of total above-ground woody biomass versus stand age for each treatment ($R^2 = 0.99$ for both control and fertilized plots). Using these relationships, we estimated mean woody biomass as 38·3 and 88·4 $m^3\ ha^{-1}$ for the control and fertilized

plots, respectively, for the experimental blocks in which measurements were made. We then estimated the vertical woody biomass distribution by scaling the total woody volume according to the woody biomass profile reported for *Pinus taeda* by Pataki, Oren & Phillips (1998).

Soil moisture measurements

Volumetric soil moisture content (θ) was measured by transects of automated time domain reflectometry (TDR) probes (Theta Probe; Delta-T Devices, Cambridge, UK) placed at two depths for each treatment plot. Two sets of five TDR probes were installed horizontally at 10 and 30 cm below ground surface. The variability in the depth-averaged θ computed from this soil moisture measurement array was small, with measured mean = 0·052 and 0·045 $m^3\ m^{-3}$ at $z = -10$ and -30 cm for the fertilized plot, and 0·047 and 0·048 $m^3\ m^{-3}$ at the two corresponding depths for the control plot.

RESULTS

To quantify the effects of fertilization on *NEE*, it is convenient to decompose *NEE* into its two primary components,

$$NEE = R_E + \int_0^h S_c(z)\,dz$$

where R_E is ecosystem respiration, and S_c are sources or sinks of CO_2 from a canopy layer of thickness dz at elevation z from the forest floor (see Fig. 1). In this study, the sign convention is negative for canopy carbon uptake by the forest.

The *CANVEG* model, which computes *NEE* from these two components, was first tested using *NEE* measurements conducted sequentially at the fertilized and the unfertilized stands. After diagnosing the model's ability to reproduce *NEE* and other biosphere-atmosphere exchange processes for this short experiment, we used the model to guide our understanding of the interplay between canopy carbon uptake and respiration from seasonal to annual time scales. These analyses permit direct contrasts of fluxes between fertilized and control stands using identical environmental conditions but different canopy physiological and structural properties.

Model validation

Figure 6 shows the comparisons between modelled and measured *NEE*, water vapour flux, and sensible heat flux for the fertilized and unfertilized plots. The sensible heat flux comparisons assess the model's ability to quantify the integrated leaf-energy balance and the modelled flow-field inside the canopy. The latent heat flux comparisons assess the ability of the model to quantify integrated stomatal conductance, and the *NEE* comparisons assess the ability of the model to reproduce net carbon exchange as the difference between photosynthesis and respiratory compo-
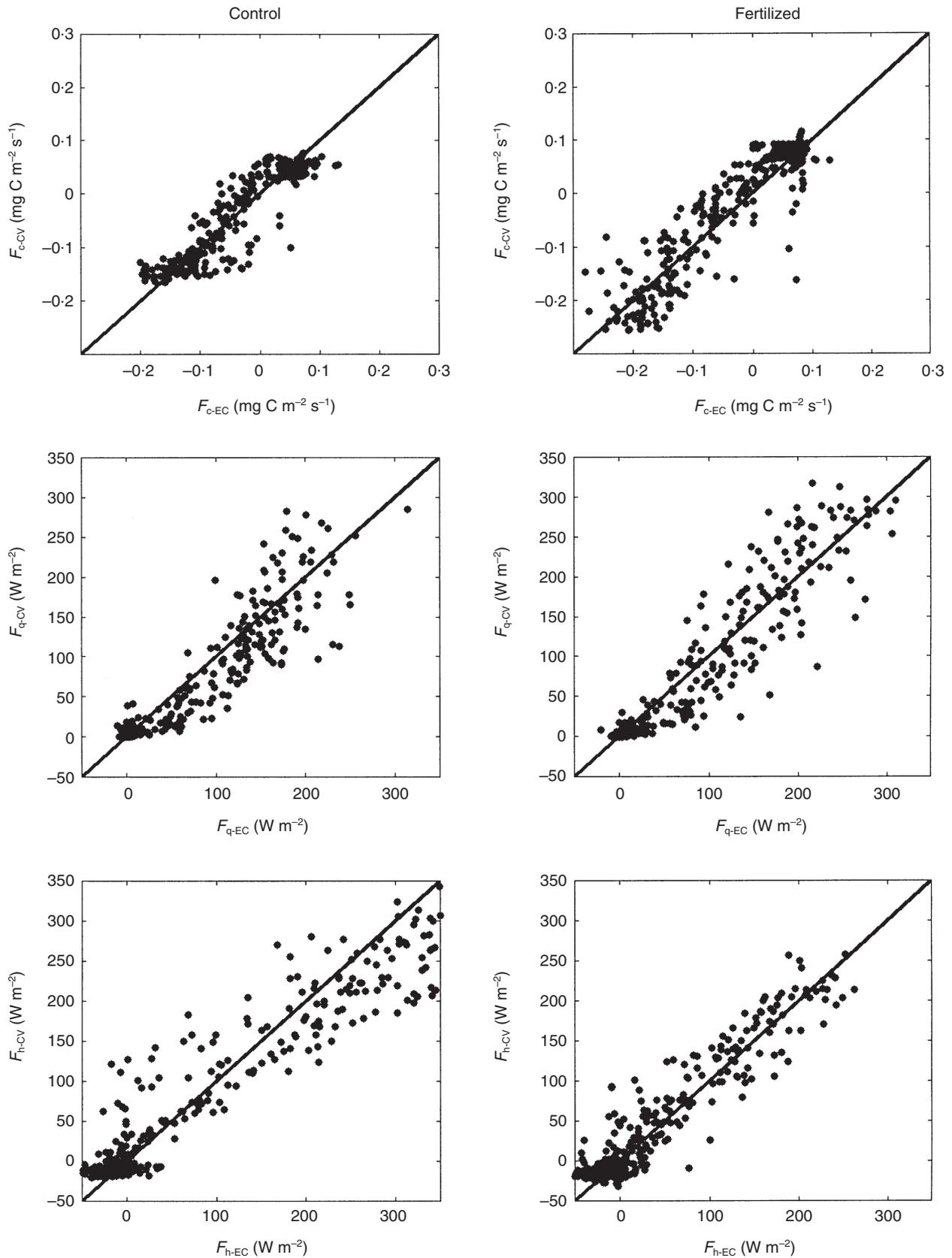
Figure 6. Comparison of CO_2 flux (F_c or *NEE*) water vapour flux (F_q) and sensible heat flux (F_T) values measured with eddy-covariance($_{EC}$) versus values modelled with *CANVEG* ($_{CV}$) at control (left column) and fertilized (right column) stands. The 1 : 1 line is also shown.

Table 2. Regression statistics for comparisons between modelled and measured fluxes of CO_2 (F_c), latent heat (F_q), and sensible heat (F_T), and mean canopy stomatal conductance (G_c) in control and fertilized stands. The linear regression model is $y = Ax + B$, where y and x are modelled and measured variables, and the coefficients A and B represent the regression slope and intercept, respectively. Also provided are coefficient of determination (R^2), root-mean square error (RMSE), and number of points in the regression analysis (N_r)

Variable	N_r	A	B	R^2	RMSE
Control					
F_c (mg C m^{-2} s^{-1})	362	0·96	−0·02	0·80	0·14
F_q (W m^{-2})	362	0·85	1·74	0·88	26·36
F_T (W m^{-2})	362	0·81	12·98	0·92	39·47
R_n (W m^{-2})	478	1·00	−1·04	0·99	21·45
G_c (mmol m^{-2} leaf s^{-1})	49	0·53	54·5	0·73	19·77
Fertilized					
F_c (mg C m^{-2} s^{-1})	391	0·98	0·03	0·83	0·17
F_q (W m^{-2})	391	0·97	−1·24	0·89	29·47
F_T (W m^{-2})	391	0·95	7·51	0·89	24·54
R_n (W m^{-2})	460	1·02	−9·82	0·98	28·40
G_c (mmol m^{-2} leaf s^{-1})	44	0·49	28·49	0·77	6·54

nents. There was good agreement between model calculations and measurements for both stands (Fig. 6, Table 2). Furthermore, the radiative transfer scheme and the associated energy balance were reproduced well by the model as is apparent from the good agreement between modelled and measured sensible heat flux and R_n (Figs 6 & 7; Table 2).

Using a parallel resistor network, an effective canopy conductance (G_c, per unit leaf area) can be computed from the *CANVEG* modelled leaf conductance $g_s(z)$ (Lai *et al.* 2000b). The response of modelled G_c to D_v was similar to that for mean canopy stomatal conductance ($= g_c$/LAI) obtained with scaled sap-flux measurements conducted at a nearby site on an older stand (Ewers, Oren & Sperry 2000), showing a linear decrease with increasing ln D_v. Using this approach, the intercept of the relationship (i.e. G_c at $D_v = 1$ kPa) can serve as a reference conductance (Oren *et al.* 1999). The reference conductance can be evaluated in relations to hydraulic constraints imposed by, for example, tree height and leaf-to-sapwood area ratio (Schäfer, Oren & Tenhunen 2000), both of which affect leaf specific hydraulic conductivity. In addition to stand age, height was also affected by fertilization, and fertilization affected leaf-to-sapwood area ratio as well. Using a simple
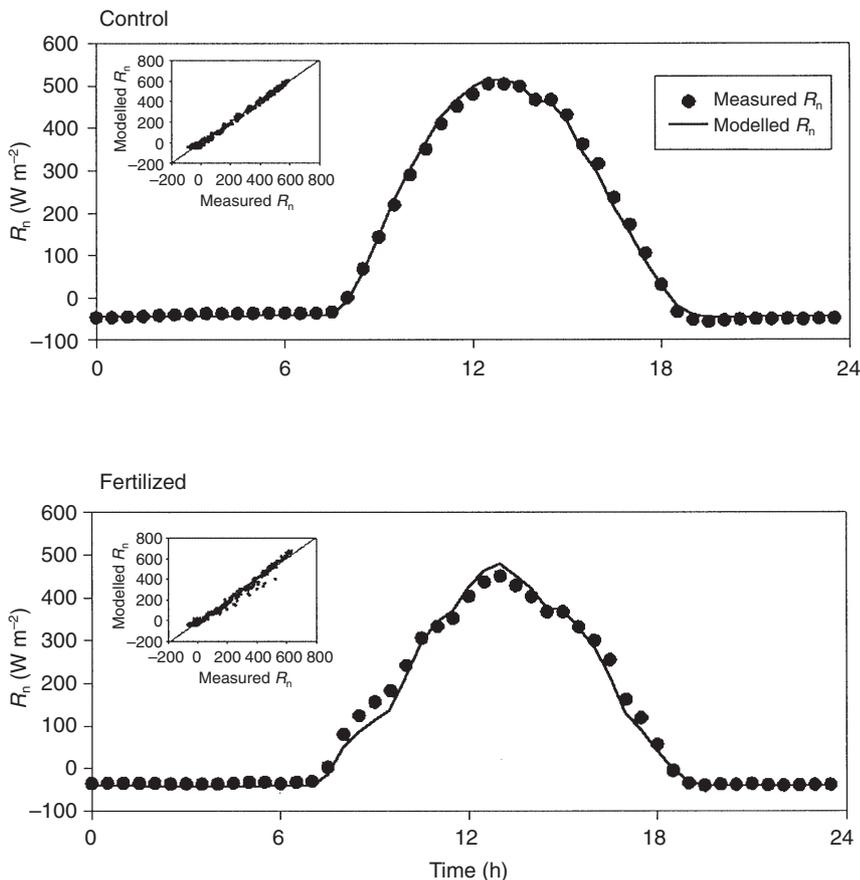

Figure 7. Comparison between modelled and measured net radiation (R_n) for control (top panel) and fertilized (bottom panel) stands.

hydraulic model (Schäfer *et al.* 2000), we estimated the theoretical rate of decrease in G_c and plotted it as a line in relation to tree height (Fig. 8a). The actual data fell quite close to the theoretical line, with the two older, taller stands showing lower G_c than the younger, shorter stands, and the
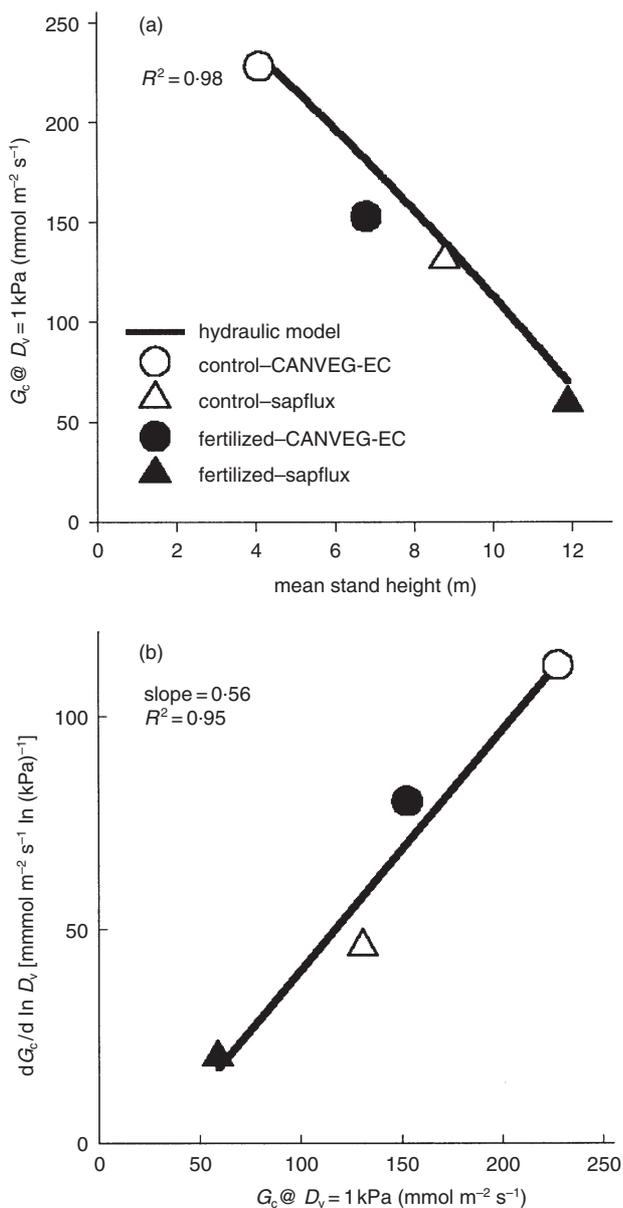

Figure 8. (a) The decrease in canopy conductance per unit leaf area (G_c) at vapour pressure deficit (D_v) of 1 kPa, as a reference conductance, with mean stand height in control and fertilized stands as compared with a trend predicted by hydraulic model that accounts for differences in canopy height and leaf area to sapwood area (see Schäfer *et al.* 2000). Model (CANVEG) combined with eddy-covariance measurements were used to estimate G_c at a 6-year-old-plantation in 2000, whereas sap-flux based estimates were obtained at a nearby stand in 1996–98 (Ewers *et al.* 2000). In (b) G_c sensitivity to D_v is assessed in relation to the reference conductance shown in (a). The expected slope of the response is ~ 0·6 (Oren *et al.* 1999).

fertilized, taller stand showing lower G_c than the unfertilized, shorter stand within the same age group. Moreover, lower leaf-to-sapwood area ratio with fertilization was sufficient to partially reverse the expected exponential decay in G_c with tree height, resulting in a nearly linear decline in both the theoretical calculations and the empirical data.

Furthermore, based on Oren *et al.* (1999), the sensitivity of G_c to D_v (i.e. $dG_c/d\ln D_v$) is directly related to G_c at $D_v = 1\,kPa$, with a theoretical slope of ~0·6, as has been found in the nearby older stand (Ewers *et al.* 2000, 2001). Again, presenting the data from all four stands show that the response of G_c to D_v was indeed proportional to G_c at $D_v = 1\,kPa$, with a slope not very different from the theoretical (Fig. 8b). We note that the data used in both analyses in Fig. 8 were obtained from long-term measurements in the two older stands and from the *CANVEG* model calculations for the two younger stands. Nevertheless, these data, which also represent different collection periods, and stands of different ages receiving different treatments and displaying a wide range in structural characteristics, seamlessly combined to show that the four stands behaved very similar to theoretical expectations. We consider this a demonstration that the model is capable to faithfully reproduce long-term stomatal behaviour.

Having demonstrated that the model is capable of reproducing all three scalar fluxes, radiative forcing above the canopy, and expected behaviour of stomata when scaled to canopy conductance, we proceeded to examine the effects of fertilization on the individual components of *NEE*.

The effects of fertilization on biosphere–atmosphere exchange

To assess the effects of fertilization, we used the measured, *RH*, *PAR*, T_a, $\bar{U}$ and CO_2 concentration for the entire 20-day period and computed the components of *NEE* in addition to the three scalar fluxes. The comparisons between fertilized and control plots are shown in Fig. 9, which shows ensemble averaged fluxes by time of day. In this period, one of the largest effects of fertilization was to double LAI (Table 1). For this 3-week period, the model results in Fig. 9 suggest that:

1 Despite the two-fold increase in LAI with fertilization, net canopy photosynthesis was enhanced by only 25%.

2 All respiratory components, including forest floor, wood, and leaf, were substantially increased by fertilization. Thus, the total ecosystem respiration, defined as the sum of these components, increased by more than 50%.

3 As a result, increased night-time respiration by all these components counterbalanced all daytime gain in photosynthesis. For this reason, differences in daily NEE between treatments were minor.

4 The 24 h latent heat flux was enhanced by more than 16% due to fertilization; this enhancement is only slightly lower than the value reported for the summer months in the nearby older stand (Ewers *et al.* 1999; data not shown).
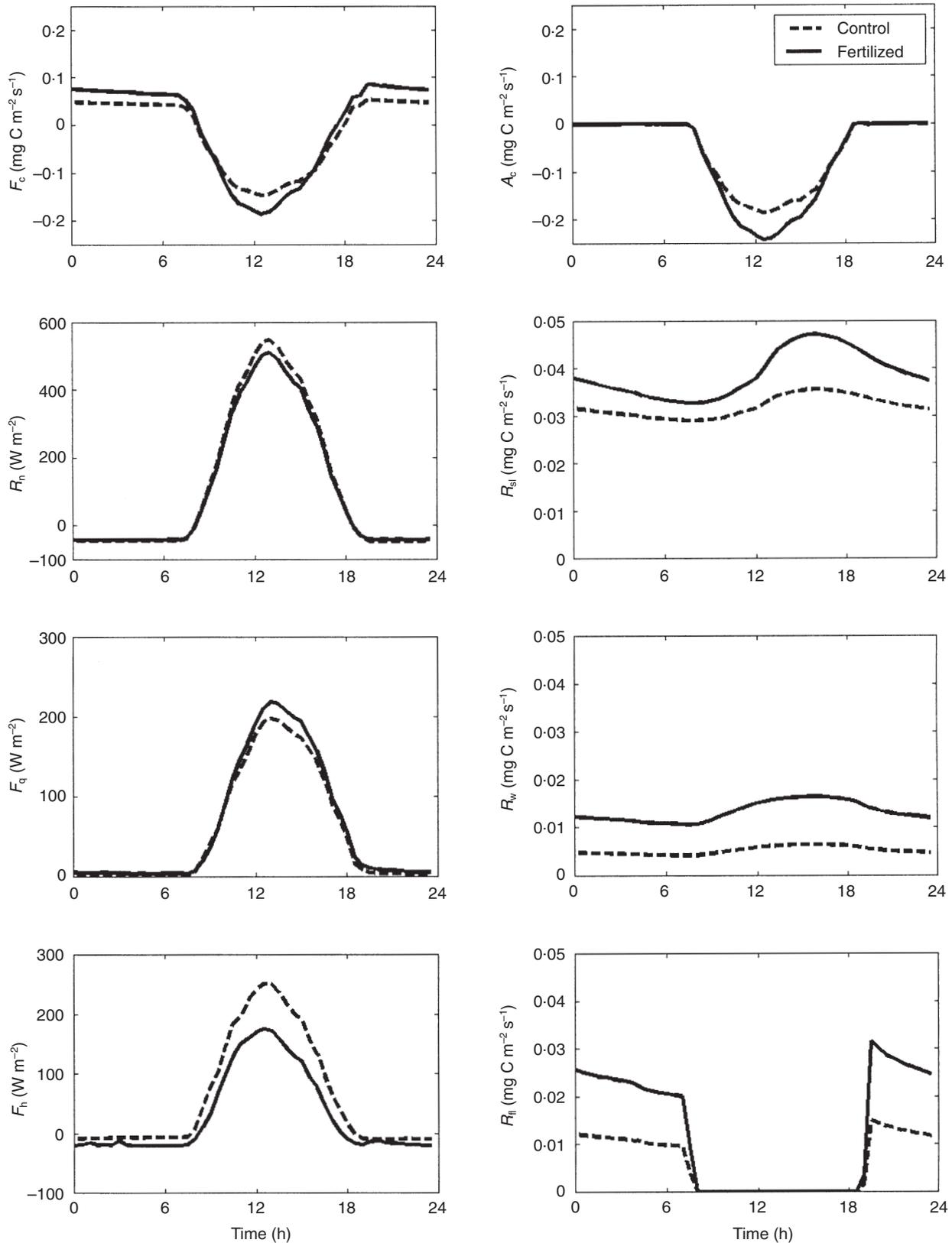
Figure 9. The effect of fertilization on modelled F_c (or *NEE*), net radiation (R_n), water vapour flux (F_q) and sensible heat flux (F_T) during the measurement period in September–October, 2000. The control (dashed) and fertilized (solid) ensemble-averages with time of day for the entire two 10-day periods are contrasted. Net canopy photosynthesis (A_c), soil respiration (R_{sl}), above-ground woody respiration (R_w) and foliar respiration (R_{fl}) differences between the two treatments is also shown as ensemble averages with time of day.
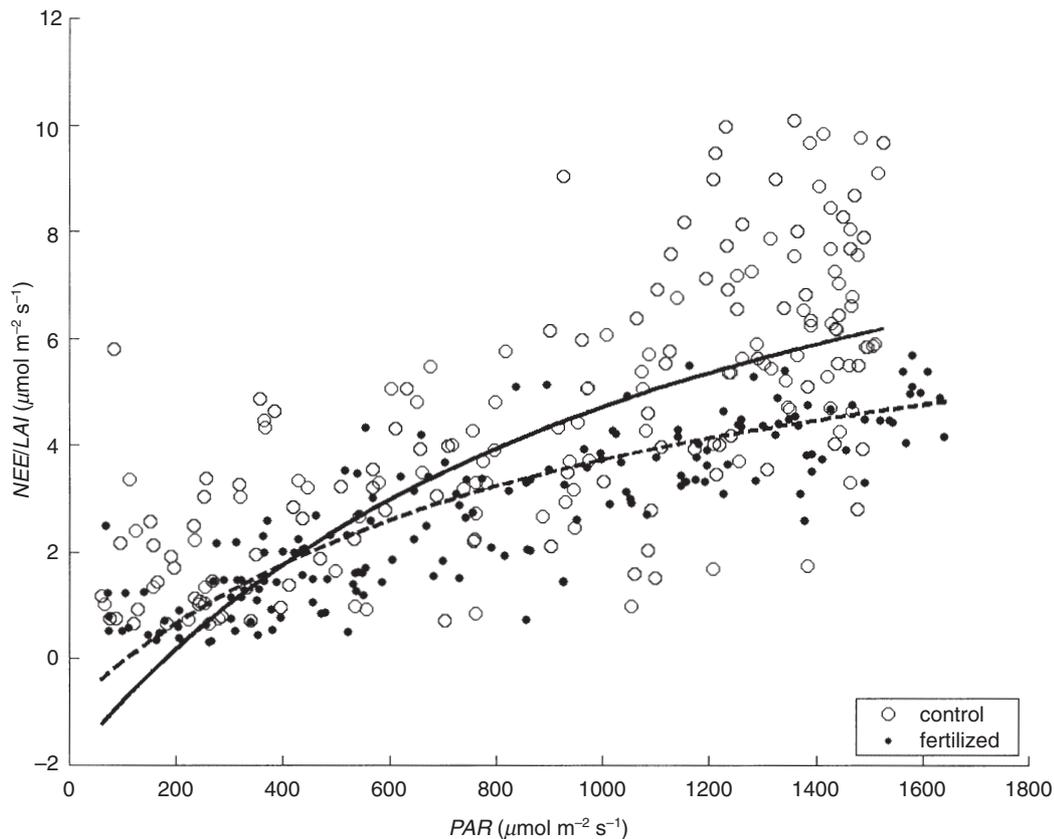
Figure 10. Variation of measured daytime Net Ecosystem Exchange (*NEE*) per unit leaf area index (LAI) with photosynthetically active radiation (*PAR*) for control and fertilized stands during the measurement period in September–October 2000.

A response curve of EC-derived ecosystem daytime *NEE*, normalized by LAI, versus light in September–October, reveals the reason for the little enhancement in net canopy photosynthesis (Fig. 10). The daytime *NEE*–light response curve was fitted to (Landsberg 1986; Ruimy *et al.* 1995)

$$NEE_d = \frac{\alpha_p \cdot PAR \cdot F_{sat}}{\alpha_p \cdot PAR + F_{sat}} - R_0$$

where NEE_d is the daytime *NEE*. Figure 10 shows the two NEE_d–*PAR* curves generated for control and fertilized plots ($R^2 = 0.49$ and 0.70, respectively). The estimated mean apparent quantum yield (α_p), net CO_2 flux at light saturation (F_{sat}), and the mean net CO_2 flux at $PAR = 0$ (R_0) for both control and fertilized plots are presented in Table 3. The large increase in LAI with fertilization reduced *NEE* per unit leaf area, especially in high *PAR*, a reduction that nearly eliminated the advantage gained in fertilized stands by having a higher LAI. Next we evaluate how the increase in LAI caused redistribution of *PAR* and scalar sources and sinks along the canopy depth such that the effect on canopy net photosynthesis was small relative to the increase in LAI.

The effects of fertilization on the vertical distribution of scalar sources and sinks

To investigate the effects of increased LAI on light transmission, photosynthesis distribution within the canopy, and

Table 3. Parameters of the response of net ecosystem exchange (*NEE*) estimated from eddy-covariance measurements to photosynthetically active radiation (*PAR*) obtained over the control and fertilized stands in September–October 2000. The parameters are: mean apparent quantum yield (α_p), net CO_2 flux at light saturation (F_{sat}), and the mean net CO_2 flux at $PAR = 0$ (R_0). For reference, we include estimates from a 17-year-old Loblolly Pine (*Pinus taeda* L.) forest in North Carolina (Lai *et al.* 2002) and a 24-year-old Slash Pine (*Pinus elliotii* var. *elliotii*) forest in Florida (Clark *et al.* 1999)

Variable	Control	Fertilized	Loblolly Pine, NC	Slash Pine, FL
α_p	0·021	0·034	0·029	0·044
F_{sat} (μmol m^{-2} s^{-1})	23·2	31·5	31·2	26·5
R_0 (μmol m^{-2} s^{-1})	3·25	3·28	3·90	4·62

in turn *NEE*, we modelled sunlit leaf area density and $\overline{C_i}/\overline{C_a}$ with height (Fig. 11). Leaf area doubled with fertilization, yet mid-day (i.e. maximum) sunlit LAI was estimated to increase by 45%, and integrated daytime sunlit LAI by only 25% (not shown in Fig. 11). The ratio of sunlit (photosynthetically effective) LAI to the total LAI was reduced from 0·63 to 0·43 due to fertilization. The modelled increase in $\overline{C_i}/\overline{C_a}$ at deeper canopy layers was a result of reduced leaf photosynthesis. When integrated with respect to height, the net canopy carbon uptake increased only slightly in the
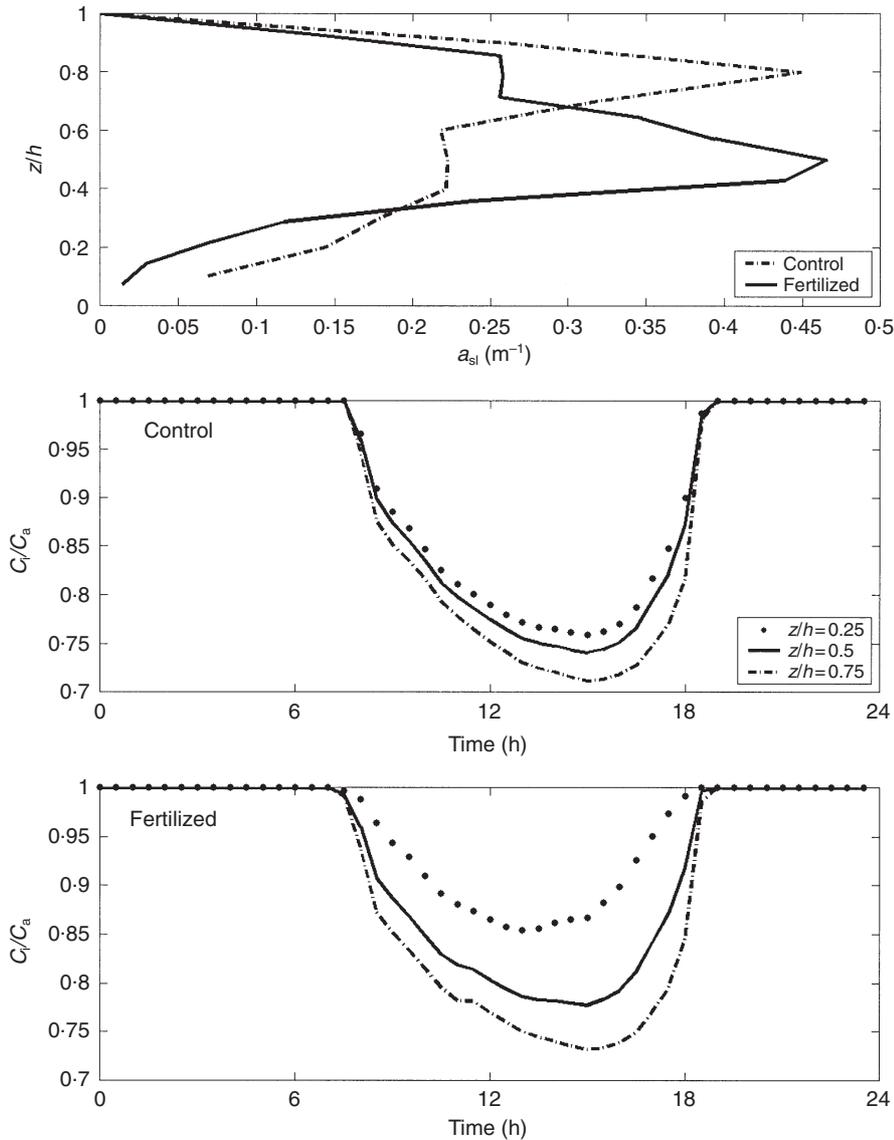
Figure 11. Comparison of midday (or maximum) sunlit leaf area density (a_{sl}) between fertilized (solid) and control (dashed) stands (top panel). Temporal variation in modelled intercellular to ambient CO_2 concentrations (C_i/C_a) at three levels within the canopy for control (middle panel) and fertilized (bottom panel) stands.

fertilized stand, which is consistent with the leaf-level findings in a *Pinus elliottii* forest (Teskey, Gholz & Cropper 1994).

Although $\overline{C_i}/\overline{C_a}$ differences between fertilized and control stands suggest changes in photosynthetic forcing variables at different levels, the vertical distribution of scalar sources is more important. These source/sink profiles, shown in Fig. 12, are calculated by accounting for differences in leaf area density (see Appendix A). Fertilization stimulated CO_2 uptake in the middle third canopy layer, just above the height of maximum a(z), but reduced uptake from the lower third canopy layer, where shading has increased. The CO_2 uptake from the top third layers was barely affected by fertilization. Similar patterns of source response are evident for water vapour. For heat, the upper 40% of the canopy realized a significant reduction in heat sources within the fertilized plots. This reduction in heat sources is due to the combined effect of lower mean wind speed and lower surface temperatures at these canopy levels. We note that maximum-modelled difference between air and surface temperatures does not exceed $0.5\,°C$, yet this gradient is sufficient to maintain an appreciable sensible heat flux. This small difference between leaf and air temperature is similar to that measured in the nearby older stand (Ewers & Oren 2000).

The effects of fertilization on respiration

The other significant response to fertilization evident from Fig. 9 is an increase in R_E. Figure 13 shows the temporal progression of R_E in fertilized versus control stands, ensemble averaged by time of day. We find that the more than 50% enhancement with fertilization in night-time respiration can offset all of the daytime gains in photosynthesis, resulting in no appreciable enhancement in *NEE* over the 3 week measurement period.
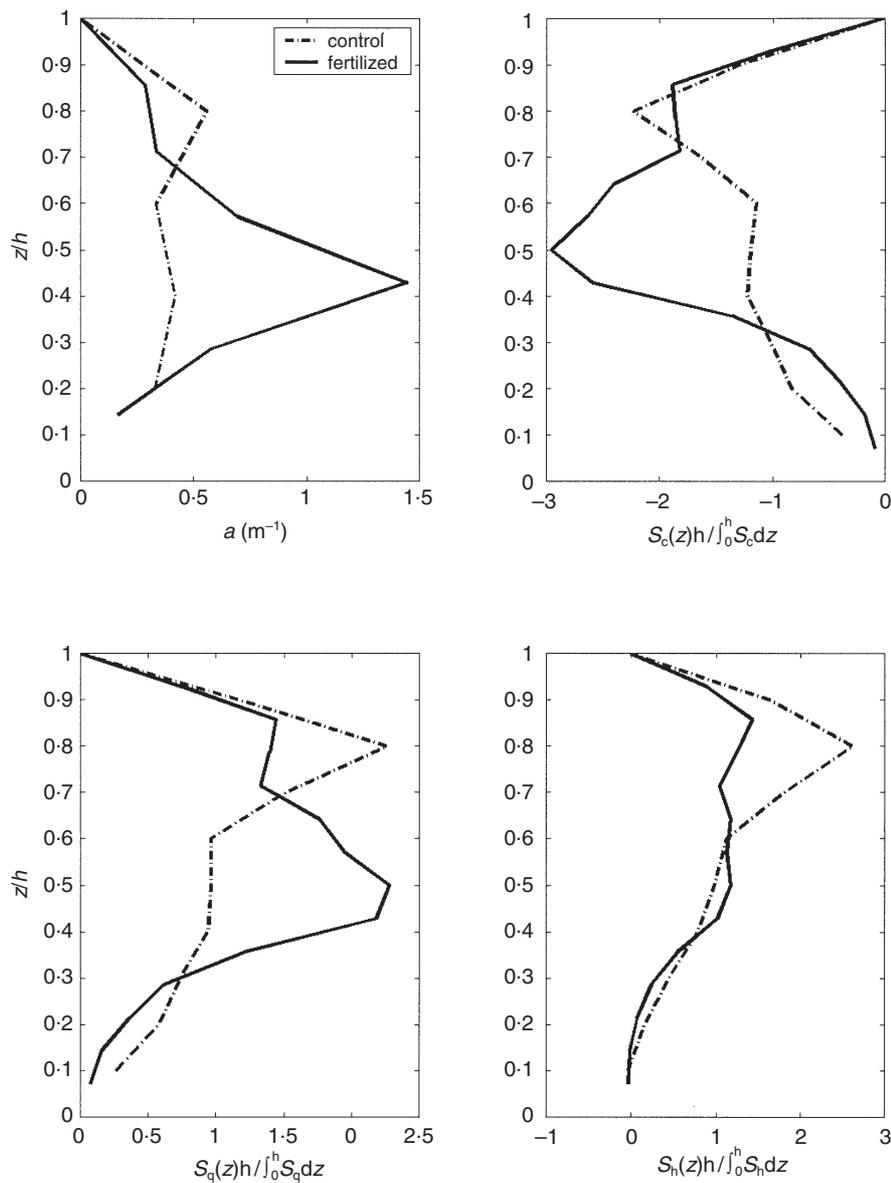
Figure 12. Fertilization-caused enhancement in the time-averaged source and sink profiles of CO_2 (S_c), water vapour (S_q), and heat (S_T) for control (dashed line) and fertilized (solid line) stands. All the source/sink profiles are normalized by their vertically integrated value at the control plots to illustrate the relative effect of fertilization. The leaf area density distribution $a(z)$ is shown for reference.

We expect these counteracting responses of increased canopy photosynthesis and respiration with fertilization, shown in Fig. 9, to be large at the end of the growing season, when LAI is near maximum and soil temperature through much of the root zone is high. However, fertilized stands at the site grow much more than unfertilized stands. We used the now tested *CANVEG* model to identify the time in the year in which the enhancement of photosynthesis with fertilization is not balanced by R_E, thus supporting greater growth.

The effects of fertilization on the annual carbon cycle

We forced the *CANVEG* model with meteorological values typical to central North Carolina, collected at Duke Forest (36°2′ N, 79°8′ W) in North Carolina (see Lai *et al.* 2000a,

b). The soil temperature measurements were corrected to account for observed differences between fertilized and control stands. These soil temperature adjustments were based on Maier & Kress (2000) who showed that monthly mean soil temperature of the control plots is usually 3–4 °C higher than that of the fertilized plots. For each month, at least 16 d (768 30 min runs) were used in the simulations to obtain a monthly mean flux. Electric power failure, lightning strikes, precipitation, and calibration runs prevented continuous measurements over the entire year.

The monthly LAI was used along with environmental drivers in the *CANVEG* model calculations. The monthly LAI was derived by scaling the LAI measurements in October with the monthly LAI variation measurements conducted in 1996 on a nearby stand with the same fertilization treatment. The LAI varied between 1·9 and 3·6 m² m⁻², and between 1·0 and 1·7 m² m⁻² for fertilized and control plots,
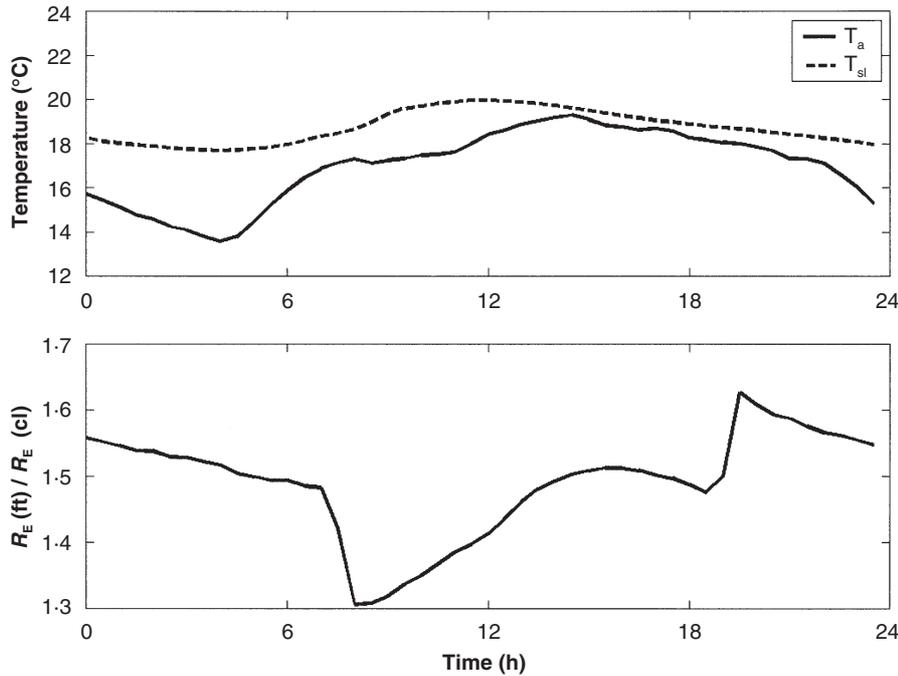
Figure 13. Enhancement of ecosystem respiration (R_E) due to fertilization for the entire two 10-day experimental periods. The ensemble-averaged air and soil temperatures are shown for reference.

respectively. Additionally, the physiological parameters in Table 1 were assumed static throughout the year. Table 4 summarizes the carbon balance for both fertilized and control stands. As a check, we compare these estimates of NEE_d to others derived by utilizing the relationships shown in Fig. 10 based on measured 30 min averaged *PAR*, monthly LAI throughout the year, and the parameters in Table 3. These two approaches represent two end members of model complexity: detailed multilevel approaches (Wang & Jarvis 1990; Williams *et al*. 1997; Baldocchi & Meyers

Table 4. Annual carbon balance for control and fertilized stands using typical meteorological conditions in central North Carolina and ecophysiological properties in Table 1. All units are in g C m^{-2} year^{-1} unless stated otherwise. The sign convention for canopy carbon uptake is negative. For differences, positive implies gain in carbon due to fertilization

Variable	Control	Fertilized	Differences	Modelled/estimated by
Gross primary productivity (GPP^1)	−1220	−1795	575	CANVEG
Respiration components				CANVEG
(i) Forest floor (R_{sl})	1107	1140	33	
(ii) Above-ground woody (R_w)	156	395	239	
(iii) Foliar (R_{fl})	63	133	70	
Total ecosystem respiration (R_E)	1326	1668	342	$R_E = R_{sl} + R_w + R_{fl}$
Net ecosystem exchange (NEE^1)	106	−127	233	$NEE^1 = GPP^1 - R_E$
Net primary production (NPP)	781	1185	602	NPP (control) $= 0{\cdot}64\ GPP^1$
				NPP (fert.) $= 0{\cdot}66\ GPP^1$
Daytime NEE (NEE_d)	−525	−993	466	NEE_d–PAR curve
Night-time R_E^{a}	695	901	206	CANVEG
NEE^2	170	−92	262	$NEE^2 = NEE_d$ −Night-time R_E
GPP^2	−1156	−1760	604	$GPP^2 = -NEE^2 + R_E$
Woody increment	121	403	282	Woody biomass increment measurements
Litterfall	117	250	133	LAI measurements
Above-ground NPP (NPP_a)	238	653	415	NPP_a = Woody increment + Litterfall
Below-ground NPP (NPP_b)	543	532	−11	$NPP_b = NPP - NPP_a$
NPP_b/NPP (%)	70	45	−25	
Autotrophic respiration (R_a)	440	610	170	$R_a = GPP^1 - NPP$
Heterotrophic respiration (R_b)	886	1058	172	$R_h = R_E - R_a$

aNight-time R_E was estimated from the modelled monthly mean respiration components by CANVEG multiplied by the length of night-time hours for each month, and then summed for the entire year.

1998) and a semi-empirical relationship (Running & Coughlan 1988; Landsberg & Waring 1997; Coops, Waring & Landsberg 1998; Cropper 2000).

DISCUSSION

The gross primary productivity ($GPP \approx$ photosynthesis in the absence of photorespiration, as discussed in Schulze, Wirth & Heimann 2000) estimated by *CANVEG* is about 1200 and 1800 $g\,C\,m^{-2}\,y^{-1}$ for the control and fertilized stands, respectively. *GPP* estimated by the semi-empirical method agree with the *CANVEG* estimate to within 2% (see Table 4). The *GPP* of the control stand is similar to the *GPP* estimated by Law, Ryan & Anthoni (1999) for a 45-year-old *Pinus ponderosa* pine forest on a sandy site in Oregon with a similar LAI (= 1·5). The *GPP* of the fertilized stand is similar to a recently reported *GPP* for a 19-year-old loblolly pine forest in North Carolina

with a similar LAI (= 3·5; Lai *et al.* 2001). Figure 14 shows that the estimated monthly *GPP* for the fertilized stand is always larger than that of the control stand. When averaged over the entire year, we find that doubling LAI by fertilization increased *GPP* only 50%, consistent with other studies (Miller 1984; Linder *et al.* 1987; Gholz *et al.* 1991).

The effects of fertilization on annual ecosystem respiration, modelled by the *CANVEG* (Table 4), are also shown on a monthly basis in Fig. 14. The enhancement due to fertilization for R_w and foliar respiration R_{fl} are 150 and 110%, respectively. The R_{sl} estimates are approximately 1100 $g\,C\,m^{-2}\,year^{-1}$ for both control and fertilized plots. The effect of fertilization on R_{sl} is not significant, consistent with previous studies in pine plantations (Cropper & Gholz 1991; Castro *et al.* 1994; Maier & Kress 2000). Of the respiratory components here, R_{sl} is the dominant contributor (> 65%) to ecosystem respiration in both stands.

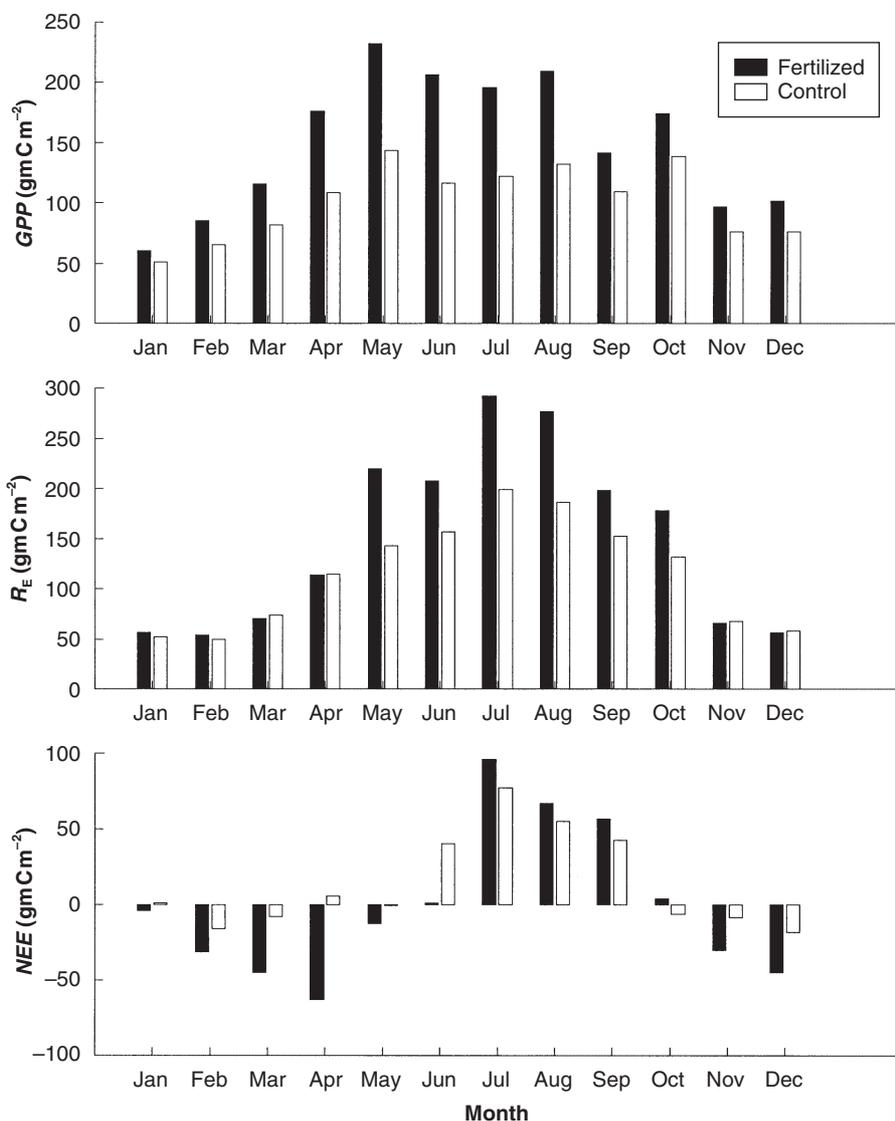**Figure 14.** Variation of modelled monthly gross primary productivity (*GPP*), ecosystem respiration (R_E) and net ecosystem exchange (*NEE*) for control and fertilized stands. The monthly *NEE* (bottom panel) is computed as $NEE = GPP - R_E$.

From estimates of *GPP* and R_E in a sparse *Pinus ponderosa* stand we calculated *NEE* near zero (Law *et al.* 1999). The results from our study (Table 4; Fig. 14) show that 6 years after planting the control stand with LAI similar to that in the *Pinus ponderosa* stand is still a week source of carbon (106 g C m^{-2} year^{-1}); however, the fertilized stand already turned into a carbon sink (–127 g C m^{-2} year^{-1}). The modelling results suggest that fertilization in poor nutrition sites shortens the time since regeneration required for pine forests to switch from an atmospheric carbon source to a sink, as proposed by Maier & Kress (2000).

On seasonal time scales, higher temperatures and increased self-shading in the summer may cause R_E to become somewhat greater than *GPP* (see Fig. 14). The consequence is a positive *NEE* (source) for both fertilized and control stands for three of the summer months. More importantly, R_E in the fertilized stand is greater than in the control stand because fertilization increased the above-ground respiratory biomass. During the non-growing season, R_E decreases more than *GPP*, but the cause of the decrease is different for each flux: lower temperature decreases R_E, whereas reduced light intensity and sunlight hours decrease *GPP*. The consequence of these reductions is a negative *NEE* (sink) in both stands, but the sink is much smaller in the control stand in spring and late autumn. Thus, based on the model results, the counteracting effects of fertilization on *NEE* measured with EC in September–October are not sustained over the entire year, and fertilization can lead to increases in *NEE*, although not in summer and early autumn months. The difference in *NEE* between fertilized and control stands during non-growing-season months more than compensates for the opposite

difference in *NEE* during the rest of the year, supporting the annual responses discussed earlier.

The modelled value of annual *NEE* for both plots is much lower than the measured above-ground net primary productivity (*NPP*). Because the stands accumulate biomass, this suggest that much of the *NPP* is supported by internal recycling of C respired in the decomposition of tissues originating in the previous stand. We investigated this possibility further by analysing the components of *GPP* further and assessing whether modelled annual *NEE* values are qualitatively reasonable.

Recent studies suggest that the ratio of net primary productivity (*NPP*) to *GPP* is approximately constant for several terrestrial ecosystems (Ryan 1991; Ryan *et al.* 1996; Williams *et al.* 1997; Waring, Landsberg & Williams 1998). Waring *et al.* (1998) found that *NPP/GPP* = 0·47 is nearly constant for 12 widely differing forested ecosystems although their assumptions leading to a constant ratio has been questioned (Medlyn & Dewar 1999). The ratio 0·47 has been adopted in simple models that estimate forest productivity from *GPP* (Landsberg & Waring 1997; Coops *et al.* 1998). Other studies found that *NPP/GPP* varies significantly with age or above-ground biomass (Mäkelä & Valentine 2001), as can be seen from a relationship of *NPP/ GPP* versus above-ground biomass (m_{ag}; Fig. 15) based on data for pine stands reported in Ryan *et al.* (1994) and Mäkelä & Valentine (2001).

Using the biomass estimates for control (684 g C m^{-2}) and fertilized (1579 g C m^{-2}) stands and based on the relationship in Fig. 15, the *NPP/GPP* for the respective stands are 0·64 and 0·59. Fertilization tends to increase *NPP/GPP* over the range of low above-ground biomass
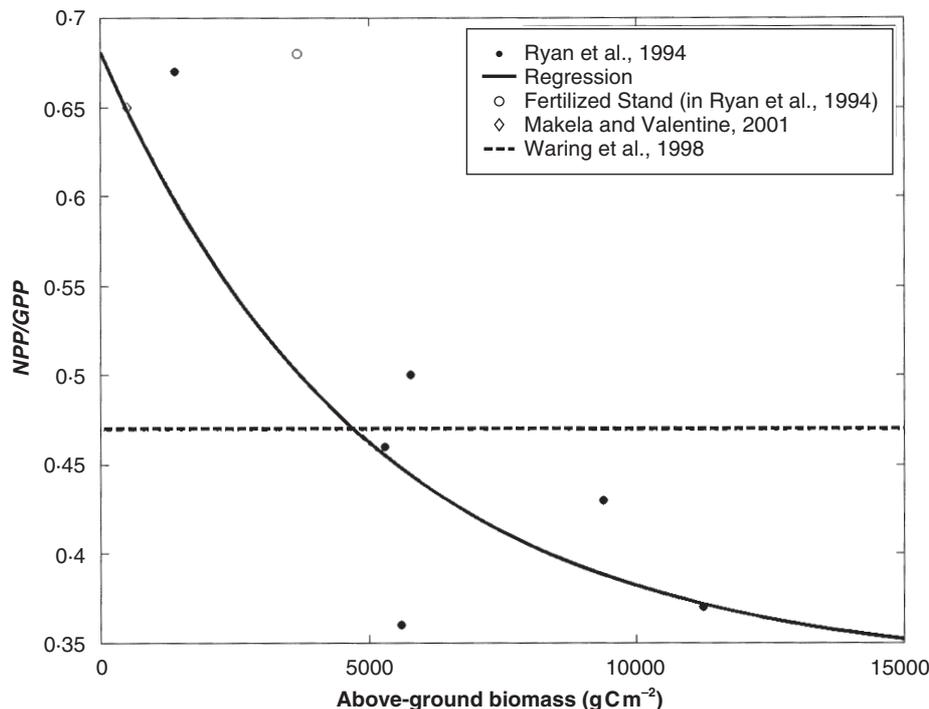

Figure 15. Variation in the ratio of net primary productivity (*NPP*) to gross primary productivity (*GPP*) in relations to above-ground biomass (m_{ag}, g C m^{-2}) for young pine stands (age < 40 years). The closed circles are measurements reported in Ryan *et al.* (1994), and the open circle is from a fertilized-irrigated *Pinus sylvestris* stand. For small above-ground biomass, we used the suggested value (diamond) in Mäkelä & Valentine (2001) derived for *P. sylvestris*. For reference, the *NPP/ GPP* = 0·47 of Waring *et al.* (1998) is shown. The solid line represents the regression fit through the unfertilized stands ($R^2 = 0·69$).

($< 4000 \, g \, C \, m^{-2}$) above its expected value ($\sim 1{\cdot}3$; Ryan *et al.* 1994; Fig. 15). Such proportional enhancement in *NPP*/*GPP* would have produced an *NPP*/*GPP* = $1{\cdot}3 \, 0{\cdot}59 = 0{\cdot}77$, which is unrealistically high, above all reported values for pines. Given that the maximum *NPP*/*GPP* for $m_{ag} < 4000 \, g \, C \, m^{-2}$ is $0{\cdot}66$, we adopted this value to reflect the effect of fertilization enhancement rather than the lower $0{\cdot}59$ that reflects the ratio of unfertilized stands. Thus, for estimating *NPP* from *GPP*, we used the following:

$$\frac{NPP}{GPP} = \begin{cases} 0{\cdot}64 \text{ (control)} \\ 0{\cdot}66 \text{ (fertilized)}, \end{cases}$$

which are higher than the mean value of $0{\cdot}47$ calculated by Waring *et al.* (1998).

Using these ratios, we estimated total *NPP* from *GPP* modelled with *CANVEG* (Table 4) as 780 and 1185 $g \, C \, m^{-2}$ for the control and fertilized stands, respectively. The below-ground portion of *NPP* (NPP_b) was then estimated by subtracting the measured above-ground *NPP* (NPP_a) from the total *NPP*. The values of estimated NPP_b were similar in both treatments (Table 4). We emphasize that the uncertainty in NPP_b is mainly due to the choice of *NPP*/*GPP*, and that small bias in the ratio can alter the estimate of NPP_b in these stands by $> 50 \, g \, C \, m^{-2}$. Nevertheless, this analysis is carried out in order to assess whether the change in carbon allocation above- and below-ground corresponds to established patterns. Although NPP_a increased by more than 170% with fertilization, modelled NPP_b/*NPP* (70 versus 45% for control and fertilized stands, see Table 4) suggests that a smaller fraction of carbon was allocated below ground in the fertilized plot. Studies on carbon allocation in trees have shown an inverse relationship between relative carbon allocation below ground and soil fertility (Santantonio 1989; Burke, Raynal & Mitchell 1992; Haynes & Gower 1995; Beets & Whitehead 1996; Van der Werf & Nagel 1996; Reynolds & D'Antonio 1996; Albaugh *et al.* 1998), and this response has been incorporated into certain growth models (Landsberg & Waring 1997). That the annual budget (Table 4) is consistent with such inverse relationship lends qualitative supports to the annual *GPP* and *NEE* modelled with CANVEG.

The measured *NPP* can be used in another independent assessment of the capability of the model to capture the effects of fertilization on annual *NEE*. Because *NPP* response to fertilization was large, yet *NEE* response was small, a pre-treatment soil organic carbon pool must have supplied through the forest floor efflux a large amount of CO_2 for assimilation. After the harvest of the previous forest in 1994, soil C content (2300 $g \, C \, m^{-2}$, Maier & Kress 2000) and the root biomass (416 $g \, C \, m^{-2}$, unpublished results from Maier) provide a rough estimate of 2700 $g \, C \, m^{-2}$ soil organic C content prior to planting. Based on 6% annual decomposition rate (Waring & Schlesinger 1985), we estimated 130 $g \, C \, m^{-2}$ of C was added to the forest floor efflux in the year 2000 from decomposition of soil organic matter carried over from the previous forest. Assuming for first-order estimate of *NEE* that root and litter turnover

rates balance their production, the atmospheric contribution to *NEE* necessary to meet the demand for above-ground woody increments (121 and 403 $g \, C \, m^{-2}$ for control and fertilized stands, see Table 4) are 9 and $-273 \, g \, C \, m^{-2}$. The annual *NEE* modelled with *CANVEG* is 106 and $-127 \, g \, C \, m^{-2}$ (Table 4), in the correct sign but approximately 100–150 $g \, C \, m^{-2}$ less negative than required in both stands. Despite the simplification and inherent errors, both *NEE* estimates suggest that the control stand is a weak source of CO_2 to the atmosphere whereas the fertilized stand is a sink.

In conclusion, fertilization increases LAI and V_{cmax}, yet the increases do not result in comparable increase in *modelled* photosynthesis or *NEE*. The results from the model show that climatic and environmental conditions in combination with greater biomass due to fertilization can increase respiration more than photosynthesis, thus diminishing fertilization-caused enhancement of *NEE*. Nevertheless, with enhanced nutrition, stands on relatively infertile soils are likely to switch earlier in the stand development from a source of, to a sink for atmospheric CO_2.

ACKNOWLEDGMENTS

REFERENCES

Albaugh T.J., Allen H.L., Dougherty P.M., Kress L.W., King J.S. (1998) Leaf area and above- and belowground growth responses of loblolly pine to nutrient and water additions. *Forest Science* **44**, 317–328.

Allen H.L. (1987) Forest fertilizers. *Journal of Forestry* **85**, 37–46.

Baldocchi D.D. & Meyers T. (1998) On using eco-physiological, micrometeorological and biogeochemical theory to evaluate carbon dioxide, water vapor and trace gas fluxes over vegetation: a perspective. *Agricultural and Forest Meteorology* **90**, 1–25.

Beets P.N. & Whitehead D. (1996) Carbon partitioning in *Pinus radiata* stands in relation to foliage nitrogen status. *Tree Physiology* **16**, 131–138.

Brix H. & Ebell L.F. (1969) Effects of nitrogen fertilization on growth, leaf area and photosynthesis rate in Douglas-fir. *Forest Science* **15**, 189–196.

Burke M.K., Raynal D.J., Mitchell M.J. (1992) Soil nitrogen availability influences seasonal carbon allocation patterns in sugar

maple (*Acer saccharum*). *Canadian Journal of Forest Research* **22**, 447–456.

Campbell G.S. & Norman J.M. (1998) *An Introduction to Environmental Biophysics*. Springer-Verlag, New York, USA.

Castro M.S., Peterjohn W.T., Melillo J.M., Steudler P.A. (1994) Effects of nitrogen fertilization on the fluxes of N_2O, CH_4, and CO_2 from soils in a Florida slash pine plantation. *Canadian Journal of Forest Research* **24**, 9–13.

Ciais P., Tans P.P., Trolier M., White J.W.C., Francey R.J. (1995) A large northern-hemisphere terrestrial CO_2 sink indicated by the C-13/C-12 ratio of atmospheric CO_2. *Science* **269**, 1098–1102.

Clark K.L., Gholz H.L., Moncrieff J.B., Cropley F., Loescher H.W. (1999) Environmental controls over net exchanges of carbon dioxide from contrasting Florida ecosystems. *Ecological Applications* **9**, 936–948.

Collatz G.J., Ball J.T., Grivet C., Berry J.A. (1991) Physiological and environmental regulation of stomatal conductance, photosynthesis and transpiration: a model that includes a laminar boundary layer. *Agricultural and Forest Meteorology* **54**, 107–136.

Coops N.C., Waring R.H., Landsberg J.J. (1998) Assessing forest productivity in Australia and New Zealand using a physiologically-based model driven with averaged monthly weather data and satellite-derived estimates of canopy photosynthetic capacity. *Forest Ecology and Management* **104**, 113–127.

Cropper W.P. Jr (2000) SPM2: a simulation model for slash pine (*Pinus elliottii*) forests. *Forest Ecology and Management* **126**, 201–212.

Cropper W.P. Jr & Gholz H.L. (1991) In situ needle and fine root respiration in mature slash pine *Pinus elliottii* trees. *Canadian Journal of Forest Research* **21**, 1589–1595.

Denmead O.T., Harper L.A., Sharpe R.R. (2000) Identifying sources and sinks of scalars in a corn canopy with inverse Lagrangian dispersion analysis. *Agricultural and Forest Meteorology* **104**, 67–73.

Evans J.R. (1989) Photosynthesis and nitrogen relationships in leaves of C3 plants. *Oecologia* **78**, 9–19.

Ewers B.E. & Oren R. (2000) Analysis of assumptions and errors in the calculation of stomatal conductance from sap flux measurements. *Tree Physiology* **20**, 579–590.

Ewers B.E., Oren R., Albaugh T.J., Dougherty P.M. (1999) Carry-over effects of water and nutrient supply on water use of *Pinus taeda*. *Ecological Application* **9**, 513–525.

Ewers B.E., Oren R., Johnsen K.H., Landsberg J.J. (2001) Estimating maximum mean canopy stomatal conductance for use in models. *Canadian Journal of Forest Research* **31**, 198–207.

Ewers B.E., Oren R., Sperry J.S. (2000) Influence of nutrient versus water supply on hydraulic architecture and water balance in *Pinus taeda*. *Plant, Cell and Environment* **23**, 1055–1066.

Fang C. & Moncrieff J.B. (1996) An improved dynamic chamber technique for measuring CO_2 efflux from the surface of soil. *Functional Ecology* **10**, 297–305.

Farquhar G.D., Von Caemmerer S., Berry J.A. (1980) A biochemical model of photosynthetic CO_2 assimilation in leaves of C_3 species. *Planta* **149**, 78–90.

Field C.B. (1991) Ecological scaling of carbon gain to stress and resource availability. In *Response of Plants to Multiple Stresses* (eds H.A. Mooney, W.E. Winner & E.J. Pell), pp. 35–65. Academic Press, San Diego, CA, USA.

Field C. & Mooney H.A. (1986) The photosynthesis-nitrogen relationship in wild plants. In *On the Economy of Plant Form and Function* (ed. T. Givnish), pp. 25–55. Cambridge University Press, Cambridge, UK.

Gholz H.L., Vogel S.A., Cropper W.P. Jr,, Mckelvey K., Ewel K.C., R.O., Curran, P.J. (1991) Dynamics of canopy structure and light interception in *Pinus elliottii* stands, north Florida. *Ecological Monographs* **61**, 33–51.

Gu L. Shugart H.H. Fuentes J.D. Black T.A. & Shewchuk S.R. (1999) Micrometeorology, biophysical exchanges and NEE decomposition in a two-story boreal forest – development and test of an integrated model. *Agricultural and Forest Meteorology* **94**, 123–148.

Haynes B.E. & Gower S.T. (1995) Below-ground carbon allocation in unfertilized and fertilized red pine plantations in northern Wisconsin. *Tree Physiology* **15** (5), 317–325.

Hirose T. & Werger M.J.A. (1987) Maximizing daily canopy photosynthesis with respect to the leaf nitrogen allocation pattern in the canopy. *Oecologia* **72**, 520–526.

Houghton R.A. Davidson E.A. & Woodwell G.M. (1998) Missing sinks, feedbacks, and understanding the role of terrestrial ecosystems in the global carbon balance. *Global Biogeochemical Cycles* **12**, 25–34.

Hsieh C.-I. Katul G., Chi, T.-W. (2000) An approximate analytical model for footprint estimation of scalar fluxes in thermally stratified atmospheric flows. *Advances in Water Research* **23**, 765–772.

Johnsen K.H. Wear D. Oren R., et al. (2001) Meeting global policy commitments: carbon sequestration and southern pine forests. *Journal of Forestry* **99**, 14–21.

Katul G.G. & Albertson J.D. (1998) An investigation of higher order closure models for a forested canopy. *Boundary Layer Meteorology* **89**, 47–74.

Katul G.G. & Chang W.H. (1999) Principal length scales in second-order closure models for canopy turbulence. *Journal of Applied Meteorology* **38**, 1631–1643.

Katul G.G., Oren R., Ellsworth D.S., Hsieh C.-I., Phillips N., Lewin K. (1997) A Lagrangian dispersion model for predicting CO_2 sources, sinks, and fluxes in a uniform loblolly pine (*Pinus taeda* L.) stand. *Journal of Geophysical Research-Atmosphere* **102**, 9309–9321.

Lai C.T., Katul G., Butnor J., Ellsworth D., Oren R. (2002) Modelling night-time ecosystem respiration by a constrained source optimization method. *Global Change Biology* **8**, 124–141.

Lai C.-T., Katul, G., Ellsworth, D.S., Oren, R. (2000a) Modeling vegetation-atmosphere CO_2 exchange by a coupled Eulerian–Lagrangian approach. *Boundary Layer Meteorology* **95**, 91–12.

Lai C.-T., Katul, G., Oren, R., Ellsworth, D., Schäfer, K. (2000b) Modeling CO_2 and water vapor turbulent flux distributions within a forest canopy. *Journal of Geophysical Research – Atmosphere* **105**, 26333–26351.

Landsberg J.J. (1986) *Physiological Ecology of Forest Production*. Academic Press, London, UK.

Landsberg J.J. & Waring R.H. (1997) A generalised model of forest productivity using simplified concepts of radiation-use efficiency, carbon balance and partitioning. *Forest Ecology and Management* **95**, 209–228.

Law B.E., Ryan M.G., Anthoni P.M. (1999) Seasonal and annual respiration of a ponderosa pine ecosystem. *Global Change Biology* **5**, 169–182.

Leuning R. (2000) Estimation of scalar source/sink distributions in plant canopies using Lagrangian dispersion analysis: corrections for atmospheric stability and comparison with a multilayer canopy model. *Boundary Layer Meteorology* **96**, 293–314.

Leuning R., Denmead O.T., Lang A.R.G. (1982) Effects of heat and water vapor transport on eddy covariance measurement of CO_2 fluxes. *Boundary Layer Meteorology* **23**, 209–222.

Leuning R., Kelliher F.M., De Pury D.G.G., Schulze E.-D. (1995) Leaf nitrogen, photosynthesis, conductance and transpiration: scaling from leaves to canopies. *Plant, Cell and Environment* **18**, 1183–1200.

Linder S. (1995) Foliar analysis for detecting and correcting nutri-

ent imbalances in Norway spruce. *Ecological Bulletins* **44**, 178–190.

Linder S., Benson M.L., Meyers B.J., Raison R.J. (1987) Canopy dynamics and growth of *Pinus radiata*. I. Effects of irrigation and fertilization during a drought. *Canadian Journal of Forest Research* **17**, 1157–1165.

Maier C.A. & Kress L.W. (2000) Soil CO_2 evolution and root respiration in 11-year-old loblolly pine (*Pinus taeda*) plantations as affected by moisture and nutrient availability. *Canadian Journal of Forest Research* **30**, 347–359.

Maier C.A., Zarnoch S.J., Dougherty P.M. (1998) Effects of temperature and tissue nitrogen of dormant season stem and branch maintenance respiration in a young loblolly pine (*Pinus taeda*) plantation. *Tree Physiology* **18**, 11–20.

Mäkelä A. & Valentine H.T. (2001) The ratio of NPP to GPP: evidence of change over the course of stand development. *Tree Physiology* **21**, 1015–1030.

McKeand S.E., Grissom J.E., Handest J.A., O'Malley D.M., Allen H.L. (2000) Responsiveness of diverse provenances of loblolly pine to fertilization – age 4 results. *Journal of Sustainable Forest* **10**, 87–94.

Medlyn B.E. & Dewar R.C. (1999) Comment on the article by R. H. Waring, J. J. Landsberg and M. Williams relating net primary production to gross primary production. *Tree Physiology* **19**, 137–138.

Miller H.G. (1984) Dynamics of nitrogen cycling in plantation ecosystems. In *Nutrition of Plantation Forests* (eds G.D. Bowen & E.K.S. Nambiar), pp. 53–78. Academic Press, London, UK.

Monteith J.L. & Unsworth M.H. (1990) *Principles of Environmental Physics* pp. 58–259. Edward Arnold, London, UK.

Murthy R., Dougherty P.M., Zarnoch S.J., Allen H.L. (1996) Effects of carbon dioxide, fertilization, and irrigation on photosynthetic capacity of loblolly pine trees. *Tree Physiology* **16**, 537–546.

Norman J.M. & Welles J. (1983) Radiative transfer in an array of canopies. *Agronomy Journal* **75**, 481–488.

Oren R., Ellsworth D.E., Johnsen K.H., *et al.* (2001) Soil fertility limits carbon sequestration by forest ecosystems in a CO_2-enriched atmosphere. *Nature* **411**, 469–472.

Oren R., Sperry J.S., Katul G.G., Pataki D.E., Ewers B.E., Phillips N., Schäfer K. (1999) Survey and synthesis of intra- and inter-specific variation in stomatal sensitivity to vapour pressure deficit. *Plant Cell and Environment* **22**, 1515–1526.

Pataki D.E., Oren R., Phillips N. (1998) Responses of sap flux and stomatal conductance of *Pinus taeda* L. trees to stepwise reductions in leaf area. *Journal of Experimental Botany* **49**, 871–878.

Pritchett W.L. & Smith W.H. (1975) Forest fertilization in the U.S. southeast. In *Forest Soils and Forest Land Management* (eds B. Bernier & C.H. Winget), pp. 467–476. Laval University Press, Quebec, Canada.

Raupach M.R. (1988) Canopy transport processes. In *Flow and Transport in the Natural Environment Advances and Applications* (eds W.L. Steffen & O.T. Denmead), pp. 95–127. Springer-Verlag, Berlin, Germany.

Raupach M.R. (1989a) A practical Lagrangian method for relating scalar concentrations to source distributions in vegetation canopies. *Quarterly Journal of Royal Meteorological Society* **115**, 609–632.

Raupach M.R. (1989b) Applying Lagrangian fluid mechanics to infer scalar source distributions from concentration profiles in plant canopies. *Agricultural and Forest Meteorology* **47**, 85–108.

Raupach M.R. & Shaw R.H. (1982) Averaging procedures for flow within vegetation canopies. *Boundary Layer Meteorology* **22**, 79–90.

Reynolds H.L. & D'Antonio C. (1996) The ecological significance of plasticity in root weight ratio in response to nitrogen: opinion. *Plant and Soil* **185**, 75–97.

Ruimy A., Jarvis P.G., Baldocchi D.D., Saugier B. (1995) CO_2 fluxes over plant canopies and solar radiation: a review. *Advances in Ecological Research* **26**, 1–28.

Running S.W. & Coughlan J.C. (1988) A general model of forest ecosystem processes for regional applications, I. Hydrologic balance, canopy gas exchange and primary production processes. *Ecological Modelling* **42**, 125–154.

Ryan M.G. (1991) A simple method for estimating gross carbon budgets for vegetation in forest ecosystems. *Tree Physiology* **9**, 255–266.

Ryan M.G., Hubbard R.M., Pongracic S., Raison R.J., McMurtrie R.E. (1996) Foliage, fine-root, woody-tissue and stand respiration in *Pinus radiata* in relation to nitrogen status. *Tree Physiology* **16**, 333–343.

Ryan M., Linder S., Vose J., Hubbard M. (1994) Dark respiration of pines. In: *Environmental Constraints on the Structure and Productivity of Pine Forest Ecosystems: a Comparative Analysis* (eds H.L. Gholz, S. Linder & R.E. McMurtrie). *Ecological Bulletins* **43**, 50–63.

Sampson D.A. & Allen H.L. (1998) Light attenuation in a 14-year-old loblolly pine stand as influenced by fertilization and irrigation. *Trees – Structure and Function* **13**, 80–87.

Samuelson L., Stokes T., Cooksey T., McLemore P. (2001) Production efficiency of loblolly pine and sweetgum in response to four years of intensive management. *Tree Physiology* **21**, 363–376.

Santantonio D. (1989) Dry-matter partitioning and fine-root production in forests – new approaches to a difficult problem. In *Biomass Production by Fast-Growing Trees* (eds J.S. Pereira & J.J. Landsberg), pp. 57–72. Kluwer Academic Publishers, Dordrecht, The Netherlands.

Schäfer K.V.R., Oren R., Tenhunen J.D. (2000) The effect of tree height on crown-level stomatal conductance. *Plant, Cell Environment* **23**, 365–377.

Schimel D.S. (1995) Terrestrial ecosystems and the carbon-cycle. *Global Change Biology* **1**, 77–91.

Schuepp P.H. (1993) Tansley review, 59: leaf boundary layers. *New Phytologist* **125**, 477–507.

Schultz R.P. (1997) *The Ecology and Culture of Loblolly Pine (Pinus taeda L.)*. USDA Agriculture Handbook 713. US Government Printing Office, Washington, DC, USA.

Schulze E.D., Wirth C., Heimann M. (2000) Managing forests after Kyoto. *Science* **289**, 2058–2059.

Siqueira M., Lai C.-T., Katul G.G. (2000) Estimating scalar sources, sinks, and fluxes in a forest canopy using Lagrangian, Eulerian, and hybrid inverse models, *Journal of Geophysical Research-Atmosphere* **105**, 29475–29488.

Tans P.P. & White J.W.C. (1998) The global carbon cycle balance, with a little help from the plants. *Science* **281**, 183–184.

Teskey R.O., Gholz H.L., Cropper J.R.W.P. (1994) Influence of climate and fertilization on net photosynthesis of mature slash pine. *Tree Physiology* **14**, 1215–1227.

Tracy C.R., van Berkum F.H., Tsuji J.S., Stevenson R.D., Nelson J.A., Barnes B.M., Huey R.B. (1984) Errors resulting from linear approximations in energy balance equations. *Journal of Thermal Biology* **9**, 261–264.

Van der Werf A. & Nagel O.W. (1996) Carbon allocation to shoots and roots in relation to nitrogen supply is mediated by cytokinins and sucrose: opinion. *Plant and Soil* **185**, 21–32.

Vitousek P.M. & Howarth R.W. (1991) Nitrogen limitation on land and in the sea – how can it occur. *Biogeochemistry* **13**, 87–115.

Vose J.M. & Allen H.L. (1988) Leaf area, stemwood growth, ad nutrition relationships in Loblolly pine. *Forest Science* **34**, 547–563.

Wang Y.P. & Jarvis P.G. (1990) Description and validation of an array model – MAESTRO. *Agricultural and Forest Meteorology* **51**, 257–280.

Waring R.H. & Schlesinger W.H. (1985) *Forest Ecosystem: Concepts and Management*, pp. 197–203. Academic Press Inc, Orlando, FL, USA.

Waring R.H., Landsberg J.J., Williams M. (1998) Net primary production of forests: a constant fraction of gross primary production? *Tree Physiology* **18**, 129–134.

Warland J.S. & Thurtell G.W. (2000) A Lagrangian solution to the relationship between a distributed source and concentration profile. *Boundary Layer Meteorology* **96**, 453–471.

Webb E.K., Pearman G.I., Leuning R. (1980) Correction of flux measurements for density effects due to heat and water vapour transfer. *Quarterly Journal of Royal Meteorological Society* **106**, 85–100.

Williams M., Rastetter E.B., Fernades D.N., *et al.* (1996) Modeling the soil-plant-atmosphere continuum in a *Quercus-Acer* stand at Harvard Forest: the regulation of stomatal conductance by light, nitrogen and soil/plant hydraulic properties. *Plant, Cell, and Environment* **19**, 911–927.

Williams M., Rastetter E.B., Fernandes D.N., Goulden M.L., Shaver G.R., Johnson L.C. (1997) Predicting gross primary productivity in terrestrial ecosystems. *Ecological Applications* **7**, 882–894.

Wilson N.R. & Shaw R.H. (1977) A higher order closure model for canopy flow. *Journal of Applied Meteorology* **16**, 1198–1205.

Wullschleger S.D. (1993) Biochemical limitations to carbon assimilation in C3 plants – a retrospective analysis of the A/C$_i$ curves from 109 species. *Journal of Experimental Botany* **44**, 907–920.

APPENDIX A. THE CANVEG MODEL FORMULATION

The basic conservation equations and parameterization schemes used in CANVEG are reviewed below.

A.1 Scalar mass balance

For a horizontally uniform and rigid canopy, the time and horizontally averaged one-dimensional scalar mass conservation equations for carbon dioxide (CO_2), water vapour, and heat, can be written as:

$$\frac{\partial \overline{C}_a}{\partial t} + \frac{\partial F_c}{\partial z} = S_c$$

$$\frac{\partial \overline{q}_a}{\partial t} + \frac{\partial F_q}{\partial z} = S_q \qquad \text{(A1)}$$

$$\frac{\partial \overline{T}_a}{\partial t} + \frac{\partial F_T}{\partial z} = S_T$$

where, $\overline{C}_a$, $\overline{q}_a$ and $\overline{T}_a$, are the mean air CO_2, water vapour concentration and temperature, respectively, F_c, F_q, F_T are the mean vertical fluxes of CO_2, water vapour and heat, and S_c, S_q, and S_T are vegetation source strength of CO_2, water vapour, and heat, respectively, t is time, and z is height above the forest floor. Mean quantities are subject to both time and horizontal averaging as discussed in Raupach & Shaw (1982). Equation A1 represents three equations with nine unknowns necessitating additional formulations to solve for, F_c, F_q, F_T, S_c, S_q and S_T.

A.2 Turbulent transport

The required additional formulations can be derived from the relationship between source strength and mean concentration via Lagrangian fluid mechanics principles. A set of prognostic equations describing the relationship between concentration and source (or sink) for CO_2, water vapour and temperature is:

$$\overline{C}_a = \frac{1}{\rho} \int\int P(z,t;z_0,t_0) S_c(z_0,t_0) dz_0 t_0$$

$$\overline{q}_a = \frac{1}{\rho} \int\int P(z,t;z_0,t_0) S_q(z_0,t_0) dz_0 t_0 \qquad \text{(A2)}$$

$$\overline{T}_a = \frac{1}{\rho} \int\int P(z,t;z_0,t_0) S_T(z_0,t_0) dz_0 t_0$$

where ρ is the mean air density, and $P(z,t; z_0,t_0)$ is the transition probability density function determined from measured or modelled turbulent flow statistics within the canopy volume as described in Raupach (1988). For practical estimation of $P(z,t; z_0,t_0)$, Lagrangian analytical models were developed and tested for a wide range of vegetation types (Raupach 1989a, b; Warland & Thurtell 2000). In particular, the localized near field theory (LNF) proposed by Raupach (1989a, b) proved to be a parsimonious model for such applications (Katul *et al.* 1997; Gu *et al.* 1999; Denmead, Harper & Sharpe 2000; Leuning 2000; Siqueira, Lai & Katul 2000).

In this study, we used LNF theory to characterize canopy turbulent scalar dispersion or $P(z,t; z_0,t_0)$ modified to include atmospheric stability effects using the approach in Leuning (2000). The within-canopy flow statistics required for the LNF calculations were modelled using second-order closure principles (Wilson & Shaw 1977; Katul & Albertson 1998; Katul & Chang 1999). These second-order closure schemes solve the conservation of mean momentum and Reynolds stress equations within the canopy, and provide the flow statistics relevant for scalar transport from measured leaf area density and estimated foliage drag coefficients. Upon combining Eqns A1 and A2, the problem of estimating, F_c, F_q, F_T, S_c, S_q and S_T is now reduced to six equations with nine unknowns and remains unsolvable. To mathematically close this problem, three additional equations describing mass transfer from leaves to the atmosphere are needed.

A.3 Scalar transfer from leaves

The scalar source strength S can be related to the atmospheric concentration by a Fickian diffusion formulation through the stomatal cavity and the leaf boundary layer. These formulations lead to the following expressions:

$$S_c(z) = -\rho a(z) \frac{\overline{C}_a(z) - \overline{C}_i(z)}{r_b(z) + r_s(z)} \tag{A3a}$$

$$S_q(z) = -\lambda_l a(z) \frac{\overline{q}_a(z) - \overline{q}_i(z)}{r_b(z) + r_s(z)} \tag{A3b}$$

$$S_T(z) = -\rho C_p a(z) \frac{\overline{T}_a(z) - \overline{T}_i(z)}{r_b(z)} \tag{A3c}$$

where subscripts a and i represent the 'free' atmosphere and subcavity space concentration values, λ_l is the latent heat of vapourization, C_p is the specific heat of dry air under constant pressure, $a(z)$ is the plant area density, $r_b(z)$ is the mean boundary layer resistance, and $r_s(z)$ is the mean stomatal resistance at a given z. For simplicity, all the symbols representing mean resistances (or conductance) are shown without overbar throughout this study. Combining Eqns A1–A3, then $\overline{C}_a$, $\overline{q}_a$, $\overline{T}_a$, F_c, F_a, F_T, S_c, S_q, and S_T can be solved if $r_b(z)$, $r_s(z)$, $\overline{C}_i$, $\overline{q}_i$ and $\overline{T}_i$ are modelled or parameterized. The modelling of $r_b(z)$, $r_s(z)$, $\overline{C}_i$, $\overline{q}_i$ and $\overline{T}_i$ is discussed next.

A.4 Resistance parameterizations: $r_b(z)$ *and* $r_s(z)$

The estimation of r_b is based on flat plate theory (Schuepp 1993; Baldocchi & Meyers 1998), but computed using the mean wind speed within the canopy, which in turn is modelled from second-order closure principles. Collatz *et al.* (1991) developed a physiological model to relate stomatal conductance g_s to leaf photosynthesis, given by

$$\frac{1}{r_s} = g_s = m \frac{A_n rh}{C_s} + b \tag{A4}$$

where m and b are species-specific parameters, determined by gas-exchange measurements, A_n is the net leaf assimilation rate, and $\overline{C}_s$ and rh are the mean CO_2 concentration and mean relative humidity at the leaf surface, respectively.

A.5 Photosynthesis and $\overline{C}_i$ parameterization

In order to calculate A_n and $\overline{C}_i$, Farquhar's biochemical model (Farquhar, Von Caemmerer & Berry 1980) is used in conjunction with the Collatz model. According to Farquhar *et al.* (1980), A_n is given by

$$A_n \approx \min \begin{Bmatrix} J_E \\ J_c \end{Bmatrix} - R_d \tag{A5}$$

where min {} denotes the minimal value among variables considered, J_E and J_c are the leaf assimilation rates constrained by electron transport capacity (J_{max}) and maximum carboxylation rate (V_{cmax}), respectively, and R_d is the respiration rate during daytime without photorespiration. The functional relationship between A_n and $\overline{C}_i$ (i.e. the A–C_i

curve) generated by gas-exchange measurements can be used to determine J_{max} and V_{cmax}, also summarized in Table 1 for the model calculation. Details of the Farquhar formulation and parameterization of J_E, J_c and R_d are given in Appendix B.

A.6 Radiative transfer

Radiation attenuation inside the canopy is critical to both the Farquhar photosynthesis model and the leaf energy budget. In our *CANVEG* model, the light transmission model of Campbell & Norman (1998) was adopted and is briefly described below.

The solar (short-wave) radiation was decomposed into direct beam, diffuse and reflective radiation as described in Campbell & Norman (1998). For thermal or long-wave radiation, the atmosphere was assumed to function as a grey body (Campbell & Norman 1998). This permits the use of an averaged sky emissivity for calculating atmospheric thermal emittance. For simplicity, we used a constant emissivity of 0·97 for the entire period.

Light transmission through the canopy is computed for sunlit and shaded portions separately to estimate *PAR* and near-infrared (NIR) irradiance absorbed at each canopy level. This waveband decomposition is necessary because leaf absorptivity is different for these two spectral bands (Monteith & Unsworth 1990; Campbell & Norman 1998).

The fraction $\tau_b(\psi)$ of incident beam radiation from a zenith angle ψ penetrating through the canopy is given by

$$\tau_b(\psi) = \exp(-\sqrt{\alpha} \, K_{be}(\psi) \, a_l \Omega) \tag{A6}$$

where α is the leaf absorptivity for *PAR*, $K_{be}(\psi)$ is the extinction coefficient for an ellipsoidal leaf distribution (see Campbell & Norman 1998), a_l () is the cumulative leaf area density integrated from the canopy top, and Ω is the clumping factor of leaf distribution ($\Omega = 1$ when leaves are randomly distributed in space). The model in Eqn A6 is sufficiently accurate if $a(z) < 0·5$ at a given layer (Norman & Welles 1983) as is the case for our study. All the radiative parameters (e.g. α and Ω) measured or assumed for this study are listed in Table 1.

A.7 Parameterization of $\overline{T}_i$, and $\overline{q}_i$: the leaf energy budget

The energy budget at the leaf surface is used to solve for surface variables (i.e. $\overline{T}_i$, and $\overline{q}_i$) and absorbed radiation for estimating g_s. Due to the strong non-linearity in the leaf energy budget, a Taylor series expansion along with a Penman approximation were used to derive an explicit algebraic equation for mean leaf surface temperature ($\overline{T}_s$), given by

$$\overline{T}_s = \overline{T}_a + \left(Q_{ab} - \lambda g_v D_v \big/ p_a - \varepsilon \sigma \overline{T}_a^4\right) \Big/$$
$$\left(h_c + \lambda g_v \Delta \big/ p_a + 4\varepsilon \sigma \overline{T}_a^3\right) \tag{A7}$$

where Q_{ab} is the absorbed energy at each canopy layer, g_v is the water vapour conductance (derived from g_s and g_b for

water vapour), D_v is the vapour pressure deficit, p_a is the atmospheric pressure, ε is the leaf emissivity, σ is the Stefan–Boltzmann constant, h_c is a convection coefficient, and Δ is the slope of the saturation vapour pressure–temperature function. The linearization in Eqn A7 is reasonable for $|\overline{T}_s - \overline{T}_a| < 2\,°C$ (Tracy *et al.* 1984), and is the case for more than 95% of the runs in this study, as was demonstrated in a similar setup by Ewers & Oren (2000).

A.8 Boundary conditions

The solution of Eqns A1–A3 requires boundary conditions at the canopy-top and at the forest floor. The upper boundary conditions are directly specified every 30 min from measured $\overline{C}_a$, $\overline{q}_a$, $\overline{T}_a$, *PAR* and $\overline{U}$. The lower boundary conditions required are F_c, F_q and F_T at $z = 0$. The latter are parameterized from a combination of measurements and simplifying assumptions. We estimated soil respiration (R_{sl}) from measured soil temperature (T_{sl}) every 30 min and a stand-specific respiration–temperature response curve. For water vapour, we assume that the forest-floor flux is about 50% of equilibrium evaporation and is estimated by

$$F_q(0,t) = \alpha_{eq} \frac{\Delta}{\Delta + \gamma} (R_n(0,t) - G_o(t))$$

with α_{eq} set to 0·5 to ensure that the soil evaporation rate does not exceed the ability of sandy soils to transmit water (estimated from the soil diffusivity for sand), γ is the psychrometric constant, G_o is the measured soil heat flux, and $F_T(0,t) = R_n(0,t) - G_o(t) - F_q(0,t)$.

APPENDIX B. PHOTOSYTHESIS MODEL (FARQUHAR *ET AL.* 1980)

Much of the following material is presented in Lai *et al.* (2000b), and thus we repeat only the key equations. According to Farquhar *et al.* (1980), the net photosynthetic rate at the leaf scale depends on light, CO_2 and leaf temperature and can be described as:

$$A_n \approx \min \begin{Bmatrix} J_E \\ J_c \end{Bmatrix} - R_d \tag{B1}$$

where J_E and J_c are the assimilation rate restricted by light and ribulose bisphosphate (RuBP) carboxylase (or Rubisco), respectively, and R_d is the respiration rate during daytime without photorespiration. In Eqn B1, J_E describes the light restriction on photosynthesis, given by:

$$J_E = \alpha \times e_m \times Q_p \frac{\overline{C}_i - \Gamma_*}{\overline{C}_i + 2\Gamma_*} \tag{B2}$$

where α is the leaf absorptivity for *PAR*, e_m is the maximum quantum efficiency for CO_2 uptake, Q_p is the *PAR* irradiance on the leaf, $\overline{C}_i$ represents mean intercellular CO_2 concentration. The CO_2 compensation point, Γ_*, is the CO_2 concentration at which $A_n = 0$ in the absence of photorespiration, and is given by:

$$\Gamma_* = \frac{[O_2]}{2\omega} \tag{B3}$$

where $[O_2]$ is the oxygen concentration in air ($\approx 210\,\text{mmol mol}^{-1}$), and ω is a ratio of kinetic parameters describing the partitioning of RuBP to the carboxylase or oxygenase reactions of Rubisco.

J_c is the Rubisco-limited rate and is estimated from:

$$J_C = \frac{V_{cmax}(\overline{C}_i - \Gamma_*)}{\overline{C}_i + K_c(1 + [O_2]/K_{o2})} \tag{B4}$$

where V_{cmax} is the maximum catalytic capacity of Rubisco per unit leaf area ($\mu\text{mol m}^{-2}\,\text{s}^{-1}$), K_c and K_{o2} are the Michaelis constants for CO_2 fixation and O_2 inhibition with respect to CO_2, respectively. Equation B4 shows that J_c increases linearly with increasing $\overline{C}_i$, , but approaches a maximum V_{cmax} under high CO_2 concentration state which is rarely encountered under natural conditions.

Following Collatz *et al.* (1991), the respiration rate R_d can be estimated by:

$$R_d = 0.015 V_{cmax} \tag{B5}$$

Temperature dependence of kinetic variables is computed following the equations in Campbell & Norman (1998). Five kinetic parameters are needed to adjust for temperature: K_c, K_o, ω, V_{cmax} and R_d. For the first three parameters, a modified Q_{10} temperature function is employed:

$$k = k_{25} \exp[y(T_s - 25)] \tag{B6}$$

where k is defined at leaf surface temperature T_s, k_{25} is the value of the parameter at 25 °C, and y is the temperature coefficient for that parameter from Campbell & Norman (1998). In addition, V_{cmax} and R_d are adjusted by a more complex function incorporating deactivation effects at extremely high temperatures, such as:

$$V_{cmax} = \frac{V_{cmax,25} \exp[0.031(T_s - 25)]}{1 + \exp[0.115(T_s - 41)]} \tag{B7}$$

and

$$R_d = \frac{R_{d,25} \exp[0.069(T_s - 25)]}{1 + \exp[1.3(T_s - 55)]} \tag{B8}$$

where $V_{cmax,25}$ and $R_{d,25}$ are the values of V_{cmax} and R_d at 25 °C, respectively.

Finally, $\overline{C}_s$, $\overline{C}_i$, and $\overline{C}_a$, are related by:

$$\overline{C}_i = \overline{C}_s - \frac{A_n}{g_s} \tag{B9}$$

and

$$\overline{C}_s = \overline{C}_a - \frac{A_n}{g_b} \tag{B10}$$

where $g_s (= r_s^{-1})$ is the stomatal conductance and $g_b (= r_b^{-1})$ is the leaf boundary layer conductance.

Appendix C. List of symbols

Symbol	Definition (units)	Comment
α	Leaf absorptivity for *PAR*	Assumed
α_p	Canopy-level quantum yield	Estimated from 30 min measured NEE_d and *PAR* above the canopy
λ_l	Latent heat of vapourization (J kg^{-1})	Assumed
Γ_*	Leaf-level mean CO_2 compensation point (p.p.m)	Modelled every 30 min
$\bar{\theta}$	Measured during intensive experiment	Depth-averaged soil moisture content every 30 min
Ω	Foliage clumping factor	Assumed
Δ	Slope of the saturation vapour pressure temperature curve (KPa °C^{-1})	
γ	Psychrometric constant	Assumed
ε	Leaf emissivity	Assumed
σ	The Stefan–Boltzmann constant	Assumed
r	Mean air density (kg m^{-3})	Modelled every 30 min
y	Zenith angle (degrees)	Modelled every 30 min
w	The ratio of kinetic parameters describing the partitioning of RuBP to the carboxylase or oxygenase reactions of Rubisco.	Assumed
$a(z)$	Leaf area density (m^2 m^{-3})	Measured during intensive experiment
$a_l(z)$	Cumulative leaf area density (m^2 m^{-2})	Measured during intensive experiment
A_n	Leaf-level photosynthesis (µmol m^{-2} s^{-1})	Modelled every 30 min
b	Intercept parameter of the Ball–Berry stomatal conductance model	Measured from porometry during intensive experiment
$\bar{C}_a$	Measured every 30 min above the canopy	Mean CO_2 concentration (p.p.m.) throughout the year
$\bar{C}_i$	Mean leaf level intercellular CO_2 concentration (p.p.m)	Modelled every 30 min
C_p	Specific heat capacity of dry air at constant pressure (J kg$^-$ K^{-1})	Assumed
D_v	Vapour pressure deficit (kPa)	Measured every 30 min above the canopy throughout the year
dt	Time increment (30 min)	
dz	Thickness of each canopy layer (m)	Set at 0·5 m
e_m	Maximum quantum efficiency for CO_2 uptake	Assumed
F_T	Sensible heat flux (W m^{-2})	Measured every 30 min during intensive experiment and modelled throughout the year
F_q	Latent heat flux (W m^{-2})	Measured every 30 min during intensive experiment and modelled throughout the year
F_c	CO_2 turbulent flux (mg C m^{-2} s^{-1})	Measured every 30 min for 10 d in each treatment and modelled for the year
F_{sat}	Net CO_2 flux at light saturation (µmol m^{-2} s^{-1})	Estimated from 30 minute measured NEE_d and *PAR* above the canopy
G_o	Soil heat flux (W m^{-2})	Measured every 30 min for 10 d in each treatment and modelled for the year
g_b	Leaf boundary layer conductance (mmol m^{-2} s^{-1})	Modelled every 30 min
g_s, G_s	Leaf and bulk canopy stomatal conductance (mmol m^{-2} s^{-1})	Modelled every 30 min
GPP	Gross primary productivity (g C m^{-2} years)	Modelled
h	Canopy height (m)	Measured
h_c	A convection coefficient	Assumed
J_c	Assimilation rate restricted by Rubisco (µmol m^{-2} s^{-1})	Modelled every 30 min
J_E	Assimilation rate restricted by light (µmol m^{-2} s^{-1})	Modelled every 30 min
J_{max}	Maximum rate of electron transport (µmol m^{-2} s^{-1})	Estimated from porometry
K_c, K_{o2}	Michaelis constants for CO_2 fixation and O_2 inhibition with respect to CO_2, respectively.	Assumed
K_o	Leaf nitrogen attenuation coefficient	Assumed
$K_{be}(\psi)$	An extinction coefficient for an ellipsoidal leaf distribution	Assumed
LAI	Leaf area index (m^2 m^{-2})	Measured and used as a model input.
m	Slope parameter of the Ball–Berry stomatal conductance model	Measured from porometry during intensive experiment
m_{ag}	above-ground biomass (g C m^{-2})	Estimated
N	Number of layers within the canopy	Set by the model
N_a	Leaf nitrogen mass (g N m^{-2})	Measured during intensive experiment.
NEE	Net ecosystem exchange in (g C m^{-2} years or mg C m^{-2} s^{-1})	Measured every 30 min for 10 d in each treatment and modelled by CANVEG every 30 min for the year
NEE_d	Daytime net ecosystem exchange (g C m^{-2} years or mg C m^{-2} s^{-1})	Same as *NEE*

Appendix C. (continued)

Symbol	Definition (units)	Comment
NPP	Net primary productivity (g C m^{-2} years)	Modelled
$[O_2]$	Mean oxygen concentration (mmol mol^{-1})	Assumed
$P(z,t; z_0,t_0)$	Probability of finding an air parcel at position z and time t knowing its original space-time position (z_0,t_0).	Modelled every 30 min
p_a	Atmospheric pressure (kPa)	Modelled from a hydrostatic approximation
PAR	Photosynthetically active radiation (μmol m^{-2} s^{-1})	Measured every 30 min above the canopy throughout the year
PAI	Plant area index (m^2 m^{-2})	Measured during the experiment
$\bar{q}_a$	Mean water vapour concentration (g kg^{-1})	Measured every 30 min above the canopy throughout the year
Q_{ab}	Absorbed energy at each canopy layer	Modelled every 30 min
Q_p	PAR irradiance on the leaf (μmol m^{-2} s^{-1})	Modelled every 30 min
R_a,R_h	Autotrophic and heterotrophic respiration rates (g C m^{-2} years)	Modelled every 30 min
R_{fl}	Foliar respiration (g C m^{-2} years)	Modelled every 30 min
R_d	Leaf dark respiration (μmol m^{-2} s^{-1})	Modelled every 30 min
R_0	Net CO$_2$ flux at $PAR = 0$ (μmol m^{-2} s^{-1})	Estimated from 30 minute measured NEE_d and PAR above the canopy
rh	Leaf relative humidity (%)	Modelled every 30 min throughout the year
RH	Mean air relative humidity (%)	Measured every 30 min throughout the year
R_E	Total ecosystem respiration (mg C m^{-2} s^{-1})	Modelled every 30 min
R_n	Net radiation (W m^{-2})	Measured every 30 min above the canopy during intensive experiment and modelled throughout the year
R_{sl}	Soil respiration (mg C m^{-2} s^{-1})	Measured every 30 min during intensive experiment and modelled from soil temperature throughout the year
R_w	Above-ground woody respiration (mg C m^{-2} s^{-1})	Measured every 30 min during intensive experiment and modelled from stem temperature throughout the year
S_c, S_q, S_T	CO$_2$, water vapour, and heat sources and sinks within the canopy (mg C m^{-3} s^{-1}, W m^{-3}, W m^{-3}), respectively.	Modelled every 30 min
t	Time (minutes, days or year)	
$\bar{T}_a$	Mean air temperature (°C)	Measured every 30 min above the canopy throughout the year
T_{sl}	Soil temperature (°C)	Measured every 30 min throughout the year
T_w	Bole temperature (°C)	Measured every 30 min throughout the year
T_s	Leaf surface temperature (°C)	Modelled every 30 min throughout the year
$\bar{U}$	Mean wind speed (m s^{-1})	Measured every 30 min above the canopy throughout the year
u^*	Friction velocity (m s^{-1})	Measured every 30 min for 10 d in each treatment and modelled for the year
V_{cmax}	Maximum carboxylation capacity (μmol m^{-2} s^{-1})	Measured from porometry during intensive experiment
V_w	Woody volume, including bark (m^3)	Measured
z	Height above forest floor (m)	